TOPOGRAPHY OPTIMIZATION OF CYLINDIRICAL SHELLS WITH CUTOUTS FOR MAXIMUM BUCKLING STRENGTH

by

Yusuf Gökyer

B.S., Metallurgical and Material Engineering, Yıldız Technical University, 2012

Submitted to the Institute for Graduate Studies in

Science and Engineering in partial fulfillment of

the requirements for the degree of

Master of Science

Graduate Program in Mechanical Engineering

Boğaziçi University

2019

TOPOGRAPHY OPTIMIZATION OF CYLINDIRICAL SHELLS WITH CUTOUTS FOR MAXIMUM BUCKLING STRENGTH

APPROVED BY:

Prof. Dr. Fazıl Önder Sönmez (Thesis Supervisor)	……
Prof. Dr. Halit S. Türkmen	……
Assoc. Prof. Çetin Yılmaz	……

DATE OF APPROVAL: 27.12.2018

ACKNOWLEDGEMENTS

I would like to express my gratitude to my supervisor Prof. Dr. Fazıl Önder Sönmez for the great remarks and engagement through the learning process of this master thesis. Working under supervision of him was a valuable experience for me and I am grateful of his patient during the period of time that I have been working on this thesis.

I am also thankful to my thesis committee members Prof. Dr. Halit S. Türkmen and Assoc. Prof. Çetin Yılmaz for spending their time to read and comment on my thesis.

ABSTRACT

TOPOGRAPHY OPTIMIZATION OF CYLINDIRICAL SHELLS WITH CUTOUTS FOR MAXIMUM BUCKLING STRENGTH

Buckling strength of shell structures under compression significantly drops if cutouts exist. In order to compensate this, these structures are reinforced with stiffeners. In this thesis, the objective is to optimize stiffener geometry and pattern on a cylindrical shell with two square holes to maximize the buckling load capacity without increase in weight.

A finite element models is developed to evaluate the buckling load of the structure. A good correlation is observed between the nonlinear analysis results of the model and the numerical and experimental results reported in the literature.

Optimization is achieved in two levels. In the first level, topography optimization is performed to obtain the optimal stiffener pattern over the shell surface based on linear eigenvalue buckling analyses. In the second level, the stiffener heights and shell thickness are optimized using a local search algorithm, Nelder-Mead. Buckling load levels are obtained by carrying out nonlinear buckling analyses in ANSYS. A PHYTON code is developed to implement the optimization method and conduct analyses in ANSYS. The results show that stiffeners need to be introduced around the cutouts and the regions near the top and bottom edges for maximum buckling load capacity. The results also reveal that stiffeners on the mid lateral surfaces of the cylinder do not make considerable contribution to buckling strength. The bucking load of the optimized stiffened geometry is 22% higher than that of the unreinforced geometry having the same weight.

ÖZET

AZAMİ BURKULMA DİRENCİ İÇİN SİLİNDİRİK DELİKLİ KABUK YAPILARDA TOPOĞRAFYA ENİYİLEMESİ

Sıkıştırma durumunda kabuk yapılarda eğer delik varsa, sıkıştırma altındaki burkulma mukavemeti önemli ölçüde düşer. Bunu telafi etmek için, bu yapılar takviye elemanları ile güçlendirilir. Bu tezde amaçlanan, ağırlık artışı olmaksızın burkulma yükü kapasitesini en üst düzeye çıkarmak için iki kare delikli silindirik bir kabuk üzerinde takviye elemanlarının geometrisini ve yerini optimize etmektir.

Yapının burkulma yükünü hesaplayabilmek için sonlu elemanlar modeli geliştirilmiştir. Modelin doğrusal olmayan analiz sonuçları ile literatürde bildirilen sayısal ve deney sonuçları karşılaştırılmış ve iyi düzeyde bir uyum gözlenmiştir.

Eniyileme iki seviyede gerçekleştirilmiştir. Birinci seviyede, doğrusal burkulma analizlerine dayanarak kabuk yüzeyi üzerinde en uygun takviye yerlerini elde etmek için topografya eniyilemesi gerçekleştirilmiştir. İkinci seviyede, takviye elemanlarının yükseklikleri ve kabuk kalınlığı, yerel bir arama algoritması olan Nelder-Mead kullanılarak optimize edilmiştir. ANSYS'te doğrusal olmayan burkulma analizleri yapılarak burkulma yük seviyelerini elde etmek, eniyileme çalışmalarını uygulamak ve ANSYS'te analiz yapmak için bir PHYTON kodu geliştirilmiştir. Sonuçlar, maksimum burkulma yükü kapasitesi için takviye elemanlarının, deliklerin ve üst ve alt kenarların yakınındaki bölgelerin etrafına yerleştirilmeleri gerektiğini göstermektedir. Sonuçlar ayrıca, silindirin orta yanal yüzeylerine yerleştirilen takviye elemanlarının burkulma kuvvetine önemli bir katkı sağlamadığını ortaya koymaktadır. Optimize edilmiş kuvvetlendirilmiş geometrinin burkulma yükü, aynı ağırlığa sahip olan kuvvetlendirilmemiş geometrininkinden % 22 daha yüksektir.

TABLE OF CONTENTS

ACKNOWLEDGEMENTS iii

ABSTRACT iv

ÖZET v

TABLE OF CONTENTS vi

LIST OF FIGURES ix

LIST OF TABLES xiii

LIST OF SYMBOLS xiv

LIST OF ACRONYMS/ABBREVIATIONS xvi

1. INTRODUCTION 1

    1.1. Motivation 1

    1.2. Literature Review 2

    1.3. Problem Statement and Objective 6

2. THEORETICAL BACKGROUND 8

    2.1. Thin-Walled Cylinders 8

        2.1.1. Stress 8

            2.1.1.1. Hoop or Circumferential Stress (σ_θ). 9

            2.1.1.2. Longitudinal or Axial Stress (σ_L). 10

            2.1.1.3. Radial Stress (σ_r). 10

        2.1.2. Changes in Dimensions 11

            2.1.2.1. Change in Length 11

            2.1.2.2. Change in Diameter 12

            2.1.2.3. Change in Internal Volume. 12

2.2. Buckling 13
2.2.1. Buckling Types 14
2.2.1.1. Nonlinear Collapse (snap-through). 14
2.2.1.2. Eigenvalue Linear Buckling 15
2.2.2. Buckling of Thin-walled Cylindrical Shells 16
3. METHODOLOGY 20
4. FE MODEL VALIDATION 24
4.1. Cylindrical Shell Geometries and Properties for Validation 24
4.2. Boundary Conditions 26
4.3. Shell-181 Element 26
4.4. Linear (Eigenvalue) and Nonlinear (Collapse) Analyses in ANSYS for Validation .. 27
4.5. Sensitivity Study for Mesh Sizing 28
4.6. Validation of the Finite Element Model 29
4.5.1. Moderately Thick Cylinder 30
4.5.2. Thin-Walled Cylinder 32
5. OPTIMIZATION STUDIES AND RESULTS 34
5.1. The Reference Cylindrical Shell 34
5.1.1. Cylindrical Shell Geometry 34
5.1.2. Finite Element Modeling 35
5.1.3. Results for the Reference Geometry 36
5.2. First Level of Optimization (Topography Optimization) 37
5.2.1. Design Constraints 39
5.2.2. Objective Function 40
5.2.3. Mesh Size, Properties and Boundary Conditions 41

5.2.4. First Level Optimization Results 41
5.3. Second Level of Optimization (Stiffener Height Optimization) 44
5.3.1. Stiffener Configuration 44
5.3.2. Stiffener Dimensions and FE modeling 46
5.4. Nelder-Mead Optimization 47
5.4.1. Objective Function 47
5.4.2. Design Variables 48
5.4.3. Design Constraints 48
5.4.4. Optimization Code 49
5.4.5. Second-Level Optimization Results 50
6. DISCUSSION 54
7. CONCLUSIONS AND FUTURE WORKS 57
REFERENCES 58

LIST OF FIGURES

Figure 1.1. (a) Stiffened interstage case in space lunch system [10], (b) GE turboprop, ATP,engine [22], (c) wing turbines' entrance door [21]. 1

Figure 1.2. Traditional types of stiffener configurations; from left to right orthogrid, angle grid, isogrid, triangle rectangle grid, respectively [20] 2

Figure 1.3. Reference geometry for optimization 7

Figure 1.4. Optimization design variables 7

Figure 2.1. Thin-walled cylinder under pressure [24]. 8

Figure 2.2. Hoop stress [24]. 9

Figure 2.3. Longitudinal stress [24]. 10

Figure 2.4. Buckling types of different structural elements. 13

Figure 2.5. Load-displacement diagram [25]. 14

Figure 2.6. Load – displacement diagram for nonlinear collapse (snap through) buckling [24]. 15

Figure 2.7. Buckled shell under axial compression [20]. 17

Figure 2.8. Cylindrical shell subjected to axial load [18]. 17

Figure 3.1. Thin-walled cylindrical shell optimization procedure..... 23

Figure 4.1. The cylindrical shell geometry used to validate the FE model. 24

Figure 4.2. Strain-Stress curve of multi-linear isotropic hardening material model in ANSYS..... 25

Figure 4.3. FE model with BC's. 26

Figure 4.4. Shell-181 element coordinate system and node locations [21]. 27

Figure 4.5. Comparison of normalized end shortening - load curves obtained by FE analysis carried out in the present study and the reference study [2]..... 30

Figure 4.6. The reference study [2]..... 31

Figure 4.7. Comparison of the experimental and numerical results of the reference study [2] and the numerical results of present study. 31

Figure 4.8. Normalized load vs end shortening plot obtained by the nonlinear analysis for L=2D and D/t = 450. 32

Figure 4.9. Normalized load vs end shortening plot obtained by the nonlinear analysis for L=5D and D/t = 450. 33

Figure 5.1. (a) Schema for the reference geometry, (b) its CAD model. 34

Figure 5.2. Meshed geometry in HYPERMESH..... 35

Figure 5.3. End shortening versus load curve for the reference geometry and von Misses stress plot (left) and the total displacement plot (right) corresponding to A, B, C points on the curve, D/t= 45, L=2D 36

Figure 5.4. The meshed geometry with green colored elements representing the design domain and orange colored elements non-design domain for the topography optimization. 38

Figure 5.5. Schematic representation of the design constraints on stiffener geometry 38

Figure 5.6. Topography optimization results obtained for different upper limits for stiffener height (a) 0.500 mm, (b) 1.00 mm, (c) 2.00 mm. 41

Figure 5.7. Topography optimization results obtained for different lower limits on stiffener width, (a) 0.625 mm, (b) 1.00 mm, (c) 2.00 mm. 42

Figure 5.8. Contour plots for different ranges of height in mm (a) 1-0.6, (b) 0.6-0.3, (c) 0.3-0. 43

Figure 5.9. (a) Front view of stiffener CAD model and topography optimization result, (b) rear view of the stiffener CAD model and the topography optimization result. 45

Figure 5.10. (a) 2D stiffener configuration, (b) 3D CAD model of the stiffeners. 45

Figure 5.11. (a) and (b) show examples of stiffener configurations in the literature [14], (c) shows the stiffener configuration on cylindrical shell in reference [10]. 46

Figure 5.12. The meshed model of the stiffened cylindrical shell in ANSYS 47

Figure 5.13. Schematic representation of the heights of the stiffeners as they are defined in the optimization code and the shell thickness. 48

Figure 5.14. The Nelder-Mead optimization procedure 49

Figure 5.15. Iteration values of the design variables and the shell thickness 51

Figure 5.16. Iteration values of the objective function (critical buckling load) 51

Figure 5.17. End shortening versus load curve for optimum stiffened geometry with von Misses stress plots corresponding to three points on the curve (A, B and C), D/t= 54.5, L=2D 53

Figure 6.1. Comparison of force versus end shortening curves for both stiffened and unstiffened geometries 56

LIST OF TABLES

Table 4.1. Dimensions of the analyzed shell geometries. 25

Table 4.2. The values for the critical buckling load calculated by the linear analysis for different mesh sizes. 29

Table 4.3. The values for the critical buckling load calculated by the nonlinear analysis for different mesh sizes.. 29

Table 4.4. Buckling loads (N) comparison, present vs. ref. study for thin shells (D/t = 450). 33

Table 5.1. Dimensions of the reference shell geometry for optimization 35

Table 5.2. Linear buckling analyses results 37

Table 5.3. The dimensions of the optimized stiffened cylinder. 52

Table 6.1. Dimensions of stiffened and unstiffened (reference) geometries 54

LIST OF SYMBOLS

A	Cross section area
a	Height of cutout
b	Width of cutout
D	Cylinder diameter
E	Young´s modulus
F	Force
H	Cylinder height
K_e	Elastic stiffness matrix
$K_{\sigma L}$	Stress matrix
L	Cylinder length
m	Buckling number of longitudinal half-waves
N_i	Initial applied load
n	Buckling number of circumferential half-waves
r	Cylinder radius
P_{cr}	Critical buckling load
p	Cylinder perimeter
S_H	Stiffener height
S_W	Stiffener width
t	Thickness
u	Deformation in x axis
V_D	Design region volume
V_S	Stiffener volume
v	Deformation in y axis
w	Deformation in z axis

δ	Deflection
ϵ_L	Axial strain
ϵ_θ	Circumferential strain
ϵ_v	Volumetric strain
λ_i	Load factor
ν	Poisson's ratio
Π	Pi value
σ_{cr}	Buckling stress
σ_L	Longitudinal (axial) stress
σ_r	Radial stress
σ_θ	Circumferential (hoop) stress
$\emptyset_i$	Eigenvector mode shape

LIST OF ACRONYMS/ABBREVIATIONS

2D	Two Dimensional
3D	Three Dimensional
ATP	Advance Turboprop
APDL	ANSYS Parametric Design Language
ASTM	American Society for Testing and Materials
BC	Boundary Condition
CAD	Computer Aided Design
DOF	Degree of Freedom
FE	Finite Element
GA	Genetic Algorithm
GE	General Electric
MPSO	Modified Particle Swarm Optimization
NASA	National Aeronautics and Space Administration

1. INTRODUCTION

1.1. Motivation

Stiffeners are secondary structural parts attached to main structure in order to make it stiffer, or more resistant to deformation, under bending loads. Increasing wall thickness is a well-known approach to improve flexural stiffness and strength, but the same stiffness and strength can be obtained by using stiffeners with a much less use of material. Stiffeners are commonly used to provide extra rigidity in such systems where weight plays critical role such as rocket launch systems, aircraft engines, aircrafts etc. NASA used a uniformly stiffened case for the interstage part of the space launch system (Figure 1.1 (a)) and GE used for the exhaust case of turboprop engine (Figure 1.1 (b)). Apart from stiffening the whole structure, sometimes stiffeners are only used to locally increase rigidity especially around cutouts that may significantly decrease the buckling strength of the structure. For example, wind-turbine towers have a considerably large hole used as entrance and stiffeners need to be used to recover the loss in the load-carrying capacity of the structure due to the cutout as shown in Figure 1.1 (c). In weight critical applications, topography and sizes of stiffeners should be judiciously chosen to make best use of stiffeners. For this purpose, a systematic methodology should be adopted to find the optimum stiffener configuration.

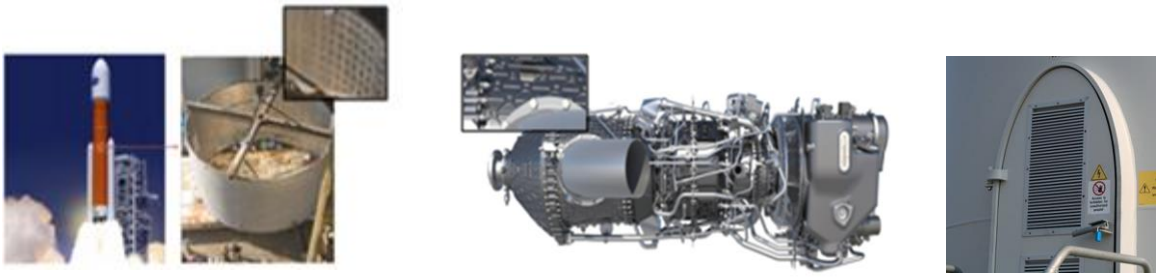

(a) (b) (c)

Figure 1.1. (a) Stiffened interstage case in space lunch system [10], (b) GE turboprop, ATP, engine [22], (c) wing turbines' entrance door [21].

1.2. Literature Review

A considerable number of researchers [3-13] studied the buckling behavior of stiffened cylindrical shells. Several researchers [14-17] interested in investigating stiffened cylinders having cutouts and aimed optimization of their geometry. In early studies [3-9], they were mainly interested in the optimization of stiffener's dimensions such as height and width and stiffeners were applied uniformly over the entire shell surface. However, in recent years, hybrid stiffener models with varying stiffener dimensions have gained importance [13, 16, 17], because more weight reduction is thus possible, but the same stiffener pattern was applied either on the entire surface or the sub-panels of shell structures. The most commonly used stiffener configurations are shown in Figure 1.2. It is worth pointing out that due to limitations of the convectional manufacturing techniques and weldability, it was not possible to produce complex stiffener patterns on shell surfaces in the past.

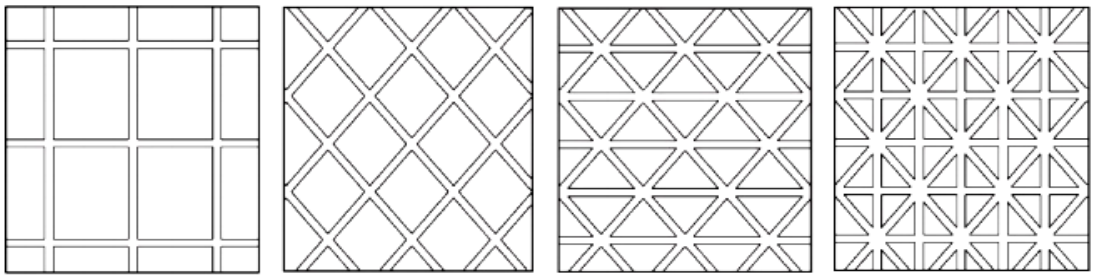

Figure 1.2. Traditional types of stiffener configurations; from left to right orthogrid, angle grid, isogrid, triangle rectangle grid, respectively [20]

Additionally, there are a great number of studies aimed to increase buckling resistance of stiffened cylindrical composite panels by optimizing stiffener cross-section, pattern, ply angle, material properties, panel thickness etc. However, because only metal cylindrical shell structures are considered in this thesis, the literature on optimization of stiffened composite structures is not discussed.

Several studies [3-10] were conducted to understand the influence of stiffener geometry on the buckling strength of cylindrical shells made of steel or aluminum with no cutouts under axial compressive loading and optimize stiffener pattern on the shell surface. Weller and Singer [3] experimentally studied the influence of stiffeners and material properties on the buckling behavior. Cylinders stiffened by stringers having different cross-sections and different spacing were tested. All tested stringer-stiffened shells provided larger buckling resistance compared to equal weight uniform shells. Hotala and Skotny [4] experimentally and numerically investigated shells having stiffeners with different shapes and lengths to increase stability and shell resistance against buckling failure. Both the results of the tests and numerical analyses show that use of short ribs interconnected with a circumferential ring highly decrease accumulation of meridional stresses and increase load-carrying capacity of such structures. Hui et al. [5] presented a theoretical study on buckling and post-buckling behavior of stiffened shells based on boundary layer theory. After examining various parameters such as shell length, thickness, stiffener cross-section etc., they pointed out that buckling behavior primarily depends on geometry of shell and stiffeners. Zhu et al. [6] presented a new design for a ring-type stiffened shell with the combination of large and small rings having T and L shape cross-sections. Optimizing the height of the stiffeners and the span of T-shaped stiffener rings under the constraint of minimum load capacity factor, buckling load-carrying capacity is maximized. Another optimization of ring stiffened shell including post-buckling behavior is provided by Forys [7] using Modified Particle Swarm Optimization (MPSO). Using several types of optimizations based on design parameters and constraining slope of post-critical path as well as material volume, the highest load critical buckling load is obtained by optimizing internal diameter and number of rings. Bagheri et al. [8] also presented optimum design of ring stiffened shell using genetic algorithm (GA). Having design variables such as shell thickness, number of stiffeners, stiffeners width and height etc. the objective functions sought the maximum fundamental frequency and minimum structural weight of shell subjected to weight, buckling load and fundamental frequency constraints. Results show that the optimized design has lower structural weight, higher natural frequency and higher buckling load carrying capacity. Sadeghifara et al. [9] investigated the optimization of cylindrical shell is stiffened by both rings and stringers. Optimization is performed varying

thickness, widths, number of both ring and stringers for rectangular, C, I, hat-shaped stiffener sections to maximize critical buckling load. It is observed that I-section and rectangular section stiffeners are, respectively, most and least efficient for stiffening shell. A study of optimizing a grid-pattern hierarchical stiffened shell for maximizing load carrying capacity under the weight constraint is examined by Wang et al. [10]. Four different types of stiffener patterns are investigated with design variables such as shell thickness and heights and number of axial and circumferential stiffener in optimization process. Higher load carrying capacity is achieved with hierarchical stiffened shell with sub-structure pattern compared to fixed pattern. Similarly, a new novel hierarchical grid stiffened design is proposed by Zhao et al. [11] based on surrogate-based optimization is adopted linear and nonlinear analysis. Structural weight was minimized under the buckling load constraint with varying shell thickness, stiffener height and number of primary and secondary axial stiffeners. Optimized hierarchical stiffened shell is lighter although it has same buckling load carrying capacity compared to the initial design. Similarly, a multi-step optimization study for hierarchical stiffened shell is published by Tian et al. [12]. Design variables are defined as width and height of primary and secondary group of stiffeners and distance of axial and vertical stiffeners and optimization is performed to maximize collapse buckling load with no weight increase. With a new design and optimization method, load-carrying capacity is increased and computational time is decreased. Hao et al. [13] obtained non-uniform optimum design of stiffeners by designing each sub-panel separately to achieve same load-carrying capacity with minimum weight. Optimizing the width and height of the stiffeners, the shell thickness, and the number of stiffeners for each sub-panel under buckling load constraint, minimum weight design is proposed.

A few numerical and experimental studies [14, 15] were conducted on stiffened cylinders with cutouts under axial compressive loading to investigate the loss of load carrying capacity due to openings and use of stiffeners were proposed to compensate this loss. Grazijahani et al. [14] studied the effect of different-size cutouts along the length of the shells in the form of wind turbine entrance door and stringer-type stiffeners welded on shell surface. Steel tubes with rectangular, elliptical, oval- shaped cutouts placed in different position on the shell surface were tested to understand load carrying capacity change based on cutout shape

and location, then I-shape stringers were welded close to cutouts. It was found that the stiffened shell with a rectangular cutout had buckling load–carrying capacity %33 higher than that of the unstiffened cylinder. Alsalah at al. [15] numerically investigated various stiffener configurations around cutouts and tried to recover buckling load-carrying capacity lost due to opening. They considered cylindrical shells made of steel with rectangular-shaped cutouts and determined the influence of shell thickness, cutout dimensions, and location on buckling load. Results showed that the cutout shape had minimal influence on the buckling load, whereas the size had much more effect. Also, it was found that frame ring configuration, where stiffeners were placed all around the cutout could fully recover of the lost capacity while the straight stiffeners were effective in recovering only 67%. Buckling load recovery capability decreased when stiffeners were placed away from the cutout.

In a few studies [16, 17], optimization of stiffened shell on cylinders with cutout was investigated to increase stiffeners' effectiveness against buckling failure. Hao et al. [16] optimized various hybrid-stiffened shell (stiffeners with various pattern and height) with a single rectangular cutout and shell with rectangular and circular cutouts. They placed different types of stiffeners on sub-panels including orthogrid, triangular grid, rotated triangular grid, and diamond grid stiffeners. Aluminum alloy structure was separated into three parts for the optimization, which are the shell itself, the weld land, and the sub-panels. Design variables for optimization were chosen as the thickness of the shell and the weld land, the width of axial weld land, the height of circumferential weld land, the stiffener height, the number of axial and circumferential stiffener cells. Cylindrical shell was simply supported at both ends and uniform compressive load was applied to the end nodes. The objective function of optimization to be minimized was defined as weight under collapse load constraint, which was to be no smaller than that of the initial design. Optimized design of hybrid-stiffened shells for both single and multiple cutouts were presented with the considerable amount of weight reduction. Another study [17] was conducted on a large, 5 m, diameter shell in a launch vehicle with multiple cutouts. A new stiffened cylindrical shell was presented based on optimizing stiffener pattern in near and far field away from the cutout locations. Multi-step optimization strategy was implemented; performing the optimization for the whole structure as

a first step to identify the dominant cutout in order to divide the structure near and far field, then perform optimization for local dominant cutout reinforcement as the second step. The numerical implementation of the asymptotic homogenization method was utilized to construct a FE model which was simply supported at the upper and lower ends and all nodes at the upper ends were coupled for uniform displacement and loading. Aluminum material properties were used for the cylindrical shell. Design variables were the number of axial and circumferential stiffeners, skin thickness, stiffener height and thickness, layout coefficients of axial and circumferential stiffeners. The objective of optimization was set to increase collapse buckling load under constraint on mass, which was not allowed to be higher than that of the initial design. Results showed that buckling usually initiated from a local region near the cutout, therefore local cutout reinforcement significantly increased the buckling load-carrying capacity of the structure.

1.3. Problem Statement and Objective

In this study, a thin-walled cylinder containing two holes is considered as shown in Figure 1.3. This structure is similar to the exhaust case with two holes connected to two pipes shown in Figure 1.1 (b). The cylinder is subjected to an axial compressive force, for this reason it is liable to buckling failure. It is well known that holes may cause significant decrease in buckling strength compared to uniform shell. Increasing thickness is not an effective way of improving buckling strength in weight critical applications compared to the use of stiffeners. For these reasons, the goal in this study is set to find the optimum topography of the stiffeners that maximizes the buckling strength of the cylindrical shell structure with cutouts. Optimization is achieved in two levels. First, topography of the stiffeners is optimized. In the second level, using the stiffener pattern determined in the first level, heights of the stiffeners and the shell thickness are optimized. The optimization variables in second level are shown in Figure 1.4.

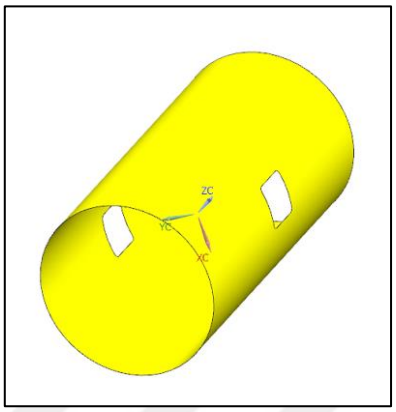

Figure 1.3. Reference geometry for optimization

In the previous studies on optimization of stiffeners on cylindrical shells, stiffener dimensions were optimized, but either stiffeners were uniformly placed on the entire surface or they were varied only by sub-panels and only few studies [16-17] considered geometrical imperfections like cutouts on shell surface and provide optimization. In the present study, on the other hand, both stiffener pattern and dimensions are optimized without differentiating the structure as sub-panels. In this study, different stiffener patterns with different heights are investigated in different regions of the cylinder with two symmetrical cutouts so that the maximum load-carrying capacity is achieved without any increase in the weight. Although, the optimum cylinder has a more complex geometry, with the help of the latest manufacturing technologies such as 3D printers, it is possible to produce complex metal structures; thus, any stiffener configuration is becoming feasible for weight reduction and better structural performance especially in aviation industry.

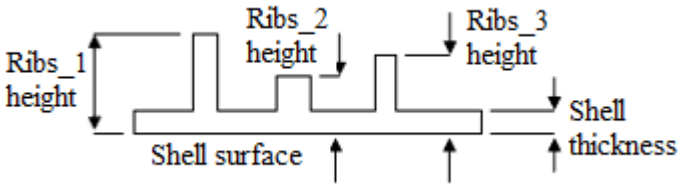

Figure 1.4. Optimization design variables

2. THEORETICAL BACKGROUND

2.1. Thin-Walled Cylinders

2.1.1. Stress

A cylinder is considered as thin walled, if it has a wall thickness equal or lower than about one- tenth of its radius, r/t >10. Three normal stresses components develop when a thin-walled cylinder is subjected to pressure;

- Hoop or circumferential stress (σ_θ)
- Longitudinal or axial stress (σ_L)
- Radial stress (σ_r)

In a thin-walled cylinder, hoop and longitudinal stresses can be assumed to constant along the thickness and radial stresses can be neglected.

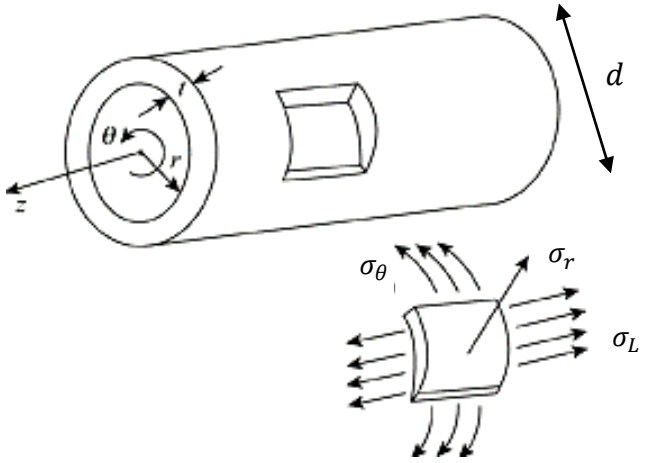

Figure 2.1. Thin-walled cylinder under pressure [24].

2.1.1.1. Hoop or Circumferential Stress (σ_θ). It is a type of mechanical stress which can be defined as results of force acting circumferentially perpendicular to both the radius and the axis. If internal pressure creates a force is more than the resisting force due to circumferential stress, structure can end up with the bursting.

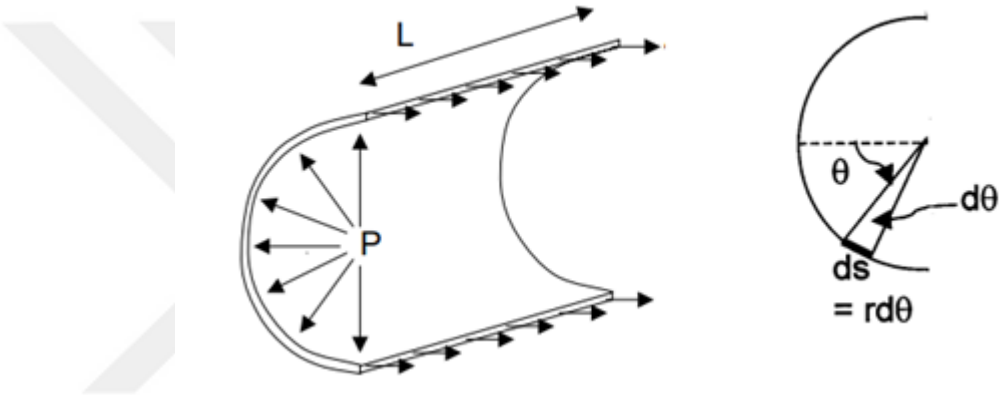

Figure 2.2. Hoop stress [24].

The forces trying to tear apart a thin-walled cylinder under pressure along a length are:

$$F = \int_{-\frac{\pi}{2}}^{\frac{\pi}{2}} prLcos\theta d\theta = 2prL = pLD \tag{2.1}$$

So long as the material holds this is balanced by the stress in the material.
The hoop stress is the force divided by cross-section area.

$$\sigma_\theta = \frac{F}{A} = \frac{pLD}{2tL} = \frac{pD}{2t} \tag{2.2}$$

2.1.1.2. Longitudinal or Axial Stress (σ_L). The stress acting along the length of the cylinder is known as longitudinal or axial stress because it acts parallel to the axis of cylinder. In this case the force on the end of the cylinder due to the pressure will be as follows

$$F = 2\int_0^r 2p\pi r dr = 2p\pi\frac{r^2}{2} = p\frac{\pi D^2}{4} \tag{2.3}$$

Since this force is acting normal to the cross-sectional area, which is approximately πDt for thin-walled cylinders, the longitudinal stress can be expressed as

$$\sigma_L = \frac{F}{A} = \frac{p\frac{\pi D^2}{4}}{\pi Dt} = \frac{pD}{4t} \tag{2.4}$$

It can be easily observed that hoop stress is two times larger than longitudinal stress.

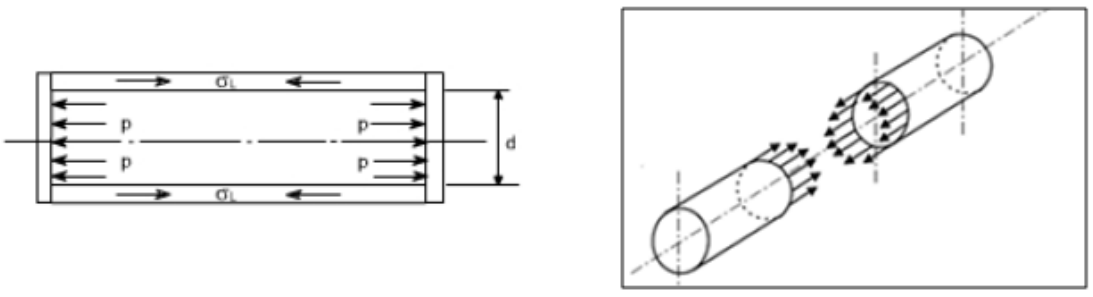

Figure 2.3. Longitudinal stress [24].

2.1.1.3. Radial Stress (σ_r). The radial stresses are normal to cylinder surface. The magnitude of radial stress is very small compared to other two stresses in thin cylinders thus it is neglected.

2.1.2. Changes in Dimensions

2.1.2.1. Change in Length. Let's take a rectangular cut from the thin-walled cylinder, there are two stresses which are axial (σ_L) and circumferential (σ_θ) and they are perpendicular to each other. Strain and stress theory defines relationship between stress and strain by using this relationship, axial strain can be

$$\epsilon_L = \frac{1}{E}(\sigma_L - \nu\sigma_\theta) \tag{2.5}$$

If calculated stresses substituted to this equation, axial strain became as

$$\epsilon_L = \frac{1}{E}\left(\frac{pD}{4t} - \nu\frac{pD}{2t}\right) = \frac{pD}{4tE}(1 - 2\nu) \tag{2.6}$$

And basically, axial strain also equal to the ratio between the change in length and its original length

$$\epsilon_L = \frac{\Delta L}{L} \tag{2.7}$$

so that formula may be written as:

$$\epsilon_L = \frac{\Delta L}{L} = \frac{1}{E}\left(\frac{pD}{4t} - \nu\frac{pD}{2t}\right) = \frac{pD}{4tE}(1 - 2\nu) \tag{2.8}$$

$$\Delta L = \frac{pD}{4tE}(1 - 2\nu)L \tag{2.9}$$

2.1.2.2. Change in Diameter. Circumferential strain simply can be expressed as

$$\epsilon_\theta = \frac{change\ in\ circumference}{original\ circumference} \tag{2.10}$$

$$\epsilon_\theta = \frac{\pi(D + \Delta D) - \pi D}{\pi D} = \frac{\Delta D}{D} \tag{2.11}$$

Using strain-stress relationship, circumferential strain is

$$\epsilon_\theta = \frac{1}{E}(\sigma_c - \nu\sigma_L) \tag{2.12}$$

Substituting both stresses, circumferential strain formula becomes as follows.

$$\epsilon_\theta = \frac{\Delta D}{D} = \frac{1}{E}\left(\frac{pD}{2t} - \nu\frac{pD}{4t}\right) = \frac{pD}{4tE}(2 - \nu) \tag{2.13}$$

$$\Delta D = \frac{pD}{4tE}(2 - \nu)D \tag{2.14}$$

2.1.2.3. Change in Internal Volume. Then volumetric strain may be expressed as

$$\epsilon_v = \frac{\Delta V}{V} = \frac{\frac{\pi(D+\Delta D)^2}{4}(L_1 + \Delta L) - (\frac{\pi D^2}{4})L_1}{\frac{\pi D^2}{4}L_1} \tag{2.15}$$

where L_1 is original length and D is diameter of thin-walled cylinder. Making simplification by ignoring the product of two small terms and dividing out, equation reduces to

(2.16)

$$\epsilon_v = \frac{\Delta L}{L_1} + 2\frac{\Delta D}{D} = \epsilon_L + 2\epsilon_c$$

Substituting stress equations, volumetric strain formula became as:

$$\epsilon_v = \frac{pD}{4tE}(5 - 4\nu) \tag{2.17}$$

$$\Delta V = \frac{pD}{4tE}(5 - 4\nu)V \tag{2.18}$$

2.2. Buckling

Buckling is failure mode that occurs when a structure suddenly undergoes a large deformation under compression. Structural instability due to a compressive force is the reason of this phenomenon is known as buckling, which causes the structure to change its shape with large displacement. Buckling failure can be catastrophic and it may cause non-utilizable products after it occurs. When the structure starts to buckle, its resistance against to initially applied force degreases significantly. The structural parts for which buckling may be critical are beams, plates, and shells. Different parts may undergo different type of buckling as shown in Figure 2.4.

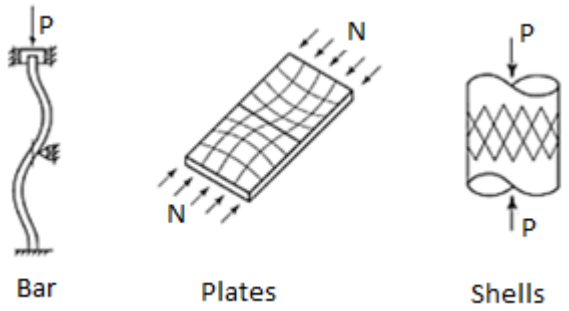

Figure 2.4. Buckling types of different structural elements [24].

The load for which a structure suddenly changes equilibrium states from stable to unstable and the applied load when structure starts to buckle at the first time known as the critical buckling load (P_{cr}) shown as critical limit point in Figure 2.5. This is point where load is largest for stability of structural element up holds in its original equilibrium configuration.

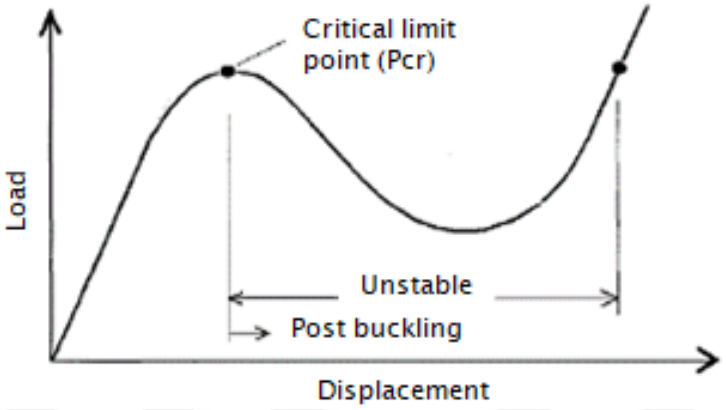

Figure 2.5. Load-displacement diagram [25].

2.2.1. Buckling Types

The type of buckling is directly related with the loading condition, structure geometry and material properties. If enough bending energy is stored in the structure during the loading, usually the nonlinear pre-buckling occurs. Based on the ratio of bending energy, there are two ways that stable structure (elastic system) turns into unstable are: nonlinear collapse (snap-through) and linear eigenvalue buckling.

2.2.1.1. Nonlinear Collapse (snap-through). Nonlinear analysis gives a chance to evaluate post-bucking behavior of the structure thus it can be obtained more information compared to linear buckling analysis. The post buckling load-deflection curves including buckling deflection is always zero before it reaches limit load for buckling and nonzero after buckling.

While the applied load increases, the strength of structure or the slope of the load-deflection curve decreases in nonlinear collapse. The slope of load-deflection curve becomes zero at the collapse load and during the structural deformation if the load is remained, buckling failure can be instantaneous and catastrophic. This type of instability failure is often called "snap-through" as shown in Figure 2.6. Nonlinear collapse can be investigated by nonlinear analysis.

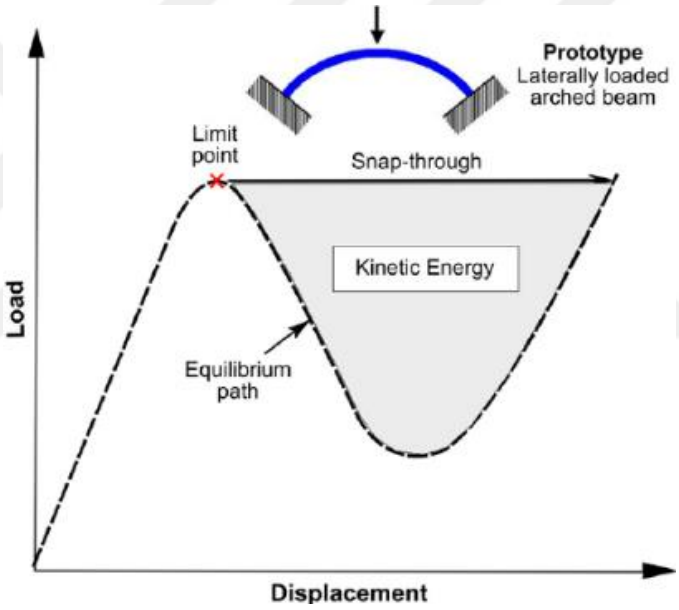

Figure 2.6. Load – displacement diagram for nonlinear collapse (snap-through) buckling [24].

The structural deformation increases in nonlinear systems while increasing the load till the neutral equilibrium point where the slope of load-displacement curve becomes zero. This point is also called limit load point, which is the maximum load structures may carry, and after this point structures snap to post-buckled state which looks like the original structure in a reversed form.

2.2.1.2. Eigenvalue Linear Buckling. Using linear eigenvalue analysis in which a eigenvalue corresponds to the buckling load level and the eigenvector corresponds to the buckling mode,

we can find general nature of buckling behavior. It is possible to know limit load by linear analysis; however, physical significance of the bifurcation buckling load cannot be known without evaluating post buckling behavior.

Also, the initial buckled shape can be found but the amplitude of the buckling deflection remains uncertain. Simply, linear bucking analysis does not predict what happens after the buckling; it can only give an idea about buckling behavior so that there is no way to evaluate post buckling behavior. Nevertheless, the linear eigenvalue analysis is a preliminary approach to solve buckling problems. Then, post buckling behavior is found with a nonlinear analysis of the equilibrium configuration after buckling.

2.2.2. Buckling of Thin-walled Cylindrical Shells

Thin-walled cylindrical shells are mostly used in various structures such as aircrafts, missiles, silos, pipelines, tanks etc. Buckling behavior of those structures is one of the problems that took the interest of many researchers and several analytical models regarding their buckling behavior are developed. Besides, structure may have large number of imperfections due to the its manufacturing process and as we discussed before, those imperfections affects load-carrying capacity of the structure. Those imperfections can be generalized as three groups:

- Geometrical: Out-of straightness and geometrical eccentricities
- Structural: Small holes, residual stresses and material inhomogeneities
- Loading imperfections: Imperfect boundary conditions, non-uniform edge load distribution, load eccentricities

Circular thin-walled cylindrical shells have imperfections which cause substantial stress concentrations and great influence. However, assuming a perfect shell without any imperfection, the classical buckling theory can be used to predict the linear buckling capacity.



Figure 2.7. Buckled shell under axial compression [20].

The analytical solution of buckling problems for thin cylindrical shells under axial pressure can be obtained as follows. If uniform axial compression force is applied on the top edge and simply supported at the ends as shown in Figure 2.8, the general solution for very small displacements can be given in the following form [18].

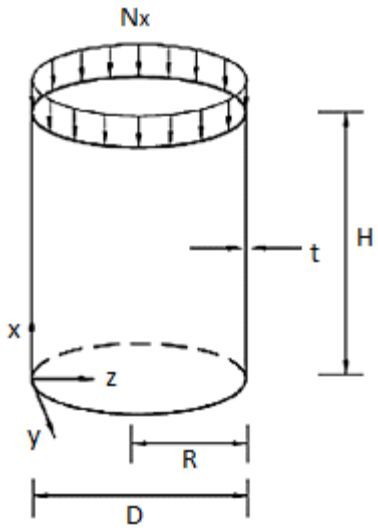

Figure 2.8. Cylindrical shell subjected to axial loading [18].

$$u = Asin(n\theta)cos\frac{m\pi x}{L}, \tag{2.19}$$

$$v = Bsin(n\theta)cos\frac{m\pi}{L}, \tag{2.20}$$

$$w = Csin(n\theta)cos\frac{m\pi x}{L} \tag{2.21}$$

where *A*, *B* and *C* are constants; *L* is the height of the cylindrical shell; and *n* and *m* are the buckling number of circumferential and longitudinal half-waves, respectively. When the simply supported conditions of $w = 0$ and $d^2w/dx^2 = 0$ are used at the ends, the critical stress is obtained as

$$\sigma_{cr} = \frac{N_X}{t} = \frac{RE}{S(1-\nu^2)} \tag{2.22}$$

$$R = (1-\nu^2)\lambda^4 + \alpha[(n^2+\lambda^2)^4 - (2+\nu)(3-\nu)\lambda^4 n^2 + 2\lambda^4(1-\nu^2) - \lambda^2 n^4(7+\nu) + \lambda^2 n^2(3+\nu) + n^4 - 2n^6] \tag{2.23}$$

$$S = \lambda^2[(n^2+\lambda^2)^2 + \frac{2}{1-\nu}\left(\lambda^2 + \frac{1-\nu}{2}n^2\right)[1+a(n^2+\lambda^2)^2] - \frac{2\nu^2\lambda^2}{1-\nu} + \frac{2a}{1-\nu}(\lambda^2 + \frac{1-\nu}{2}n^2)(n^2+(1-\nu)\lambda^2)] \tag{2.24}$$

$$a = \frac{t^2}{12R^2} \tag{2.25}$$

$$\lambda = \frac{mR\pi}{L} \tag{2.26}$$

E is Young's modulus, ν is Poisson's ratio, *t* is the thickness of the shell, and *R* is the radius of the cylinder. In theory, the critical stress calculated by Equation 2.22 has a large number of solutions based on the values of *m* and *n* and buckling stress must be the minimum critical

stress. Due to the variation of *m* and *n* values, the buckling stress becomes unknown until the enough number of critical stresses are calculated and compared in order to get the lowest critical stress that requires significant number of calculations depending on the values of *m* and *n.* Assuming that many buckling waves (*m*) form along the length of the cylinder, the value of λ^2 becomes large. Then, Equation 2.22 can be simplified as follows:

$$\sigma_{cr} = \frac{N_X}{t} = \frac{1-\nu^2}{E}\left(\alpha\frac{(n^2+\lambda^2)^2}{\lambda^2} + \frac{(1-\nu^2)\lambda^2}{(n^2+\lambda^2)^2}\right) \tag{2.27}$$

When the value of *n* in Equation 2.27 is equal to zero, axisymmetric buckling occurs, and Equation 2.26 is simplified

$$\sigma_{cr} = \frac{N_X}{t} = D\left(\frac{m^2\pi^2}{tL^2} + \frac{EL^2}{R^2Dm^2\pi^2}\right) \tag{2.28}$$

where $D=Et^3/\,[12(1-\nu^2)]$ is the flexural rigidity. Since σ_{cr} is a continuous function of mπ/H, and if the minimum value of Equation 2.28 multiplied by shell thickness, N_{cr} can be achieved from σ_{cr} in the following form which is well-known classical critical buckling load equation:

$$N_{cr} = \frac{Et^2}{R\sqrt{3(1-\nu^2)}} \tag{2.29}$$

Where *E* is Young´s Modulus, *t* is the shell thickness, *R* is the shell radius, ν is Poisson's ratio. It is found Equation 2.29 gives upper bound of experimental data if thin cylindrical shells having $H/R \leq 5$ without a cutout so it can be considered a satisfactory result on the other hand, for moderately thick shells ($R/t \leq 50$), Equation 2.29 always over estimates the capacity [2], as the shell may yield or collapse before the load reaches the predicted elastic buckling value. Another important point is that Equation 2.29 is only valid for shells of isotropic elastic materials.

3. METHODOLOGY

In this study, a finite element (FE) model is developed to study the structural behavior of stiffened cylinders with cutouts under axial compressive loading. In order to validate the FE model, comparisons are made with the numerical and experimental results reported by Han et al. [2] for both moderately thick and thin-walled cylinders with cutout under uniform axial compressive loading. Comparisons are made for two different cylinders having length/diameter ratio equal to $L/D = 2$ and 5. CAD models representing the geometric design of the cylinders are created in UNIGRAPHICS and then imported into HYPERMESH for meshing. Mesh sensitivity study is performed with various mesh sizes to find a suitable mesh size that result in reasonably small amount of error without long computational times. The meshed model is exported to ANSYS, which is used as solver for linear and nonlinear buckling analyses. The resulting load-end shortening curve for moderately thick shell is compared with numerical and experimental results in the reference study. The critical buckling load calculated using the present FE model of thin cylindrical shell is compared only with the numerically calculated load in the reference study, because no experiment was performed for the thin shell.

A moderately thick cylindrical shell with dimensions similar to the ones in the reference study is considered in this thesis for optimization. Only, the number of cutouts is two instead of one unlike the cylinder in the reference study. In this way, the cylinder bears more similarity with the aircraft exhaust case. The FE model is built in HYPERMESH using the same mesh size as the validated model. A nonlinear analysis is conducted in ANSYS to get load end-shortening curve, which is taken as the baseline/reference for the load-carrying capacity. Also, the shell mass is taken as a reference value, because it is desired to increase the load-carrying capacity by using stiffeners using the same mass as the unstiffened reference shell. For optimization purpose, the model is prepared in HYPERMESH for topography optimization in order to obtain optimum stiffener configuration on the cylinder surface under given constraints.

Optimization is achieved in two levels. In the first level, the model is then run in OPTISTRUCT and the optimum topography is obtained based on linear buckling analysis. After convergence, the stiffener pattern and width are determined based on the results of the topography optimization. In the second level of optimization, the heights of the stiffeners are optimized. Because of the cutouts, which locally weaken the structure, stiffener height is allowed to be variable. Three groups of stiffeners are chosen, then their heights and the shell thickness are optimized using a local search algorithm, Nelder-Mead to maximize the load-carrying capacity without increasing the mass. The buckling load of the configurations generated by the search algorithm during optimization is determined by conducting nonlinear finite element analysis. PHYTON code is written to integrate Nelder-Mead with ANSYS. It generates ANSYS Parametric Design Language (APDL) code to update the FE model and carries out nonlinear analysis for each configuration generated by Nelder-Mead algorithm in each iteration. Based on the critical buckling load calculated by ANSYS, the search algorithm determines the next configuration. Depending on the values of stiffener thickness provided by the algorithm, PHYTON code calculates the shell thickness such that the mass remains the same as the mass of the unstiffened shell. No upper or lower bound is defined for the variables as constraint however; the initial values of the stiffeners' heights are chosen close to the ones obtained by the topography optimization. Convergence criterion for Nelder-Mead algorithm is defined as %1, which means optimization process stops either when the differences in the values of the design variables or objective function is less than %1 for the best and the worst configurations. Via the optimization process controlled by the search algorithm, the optimum configuration with the highest critical buckling load is obtained. The optimization process is summarized in Figure 3.1.

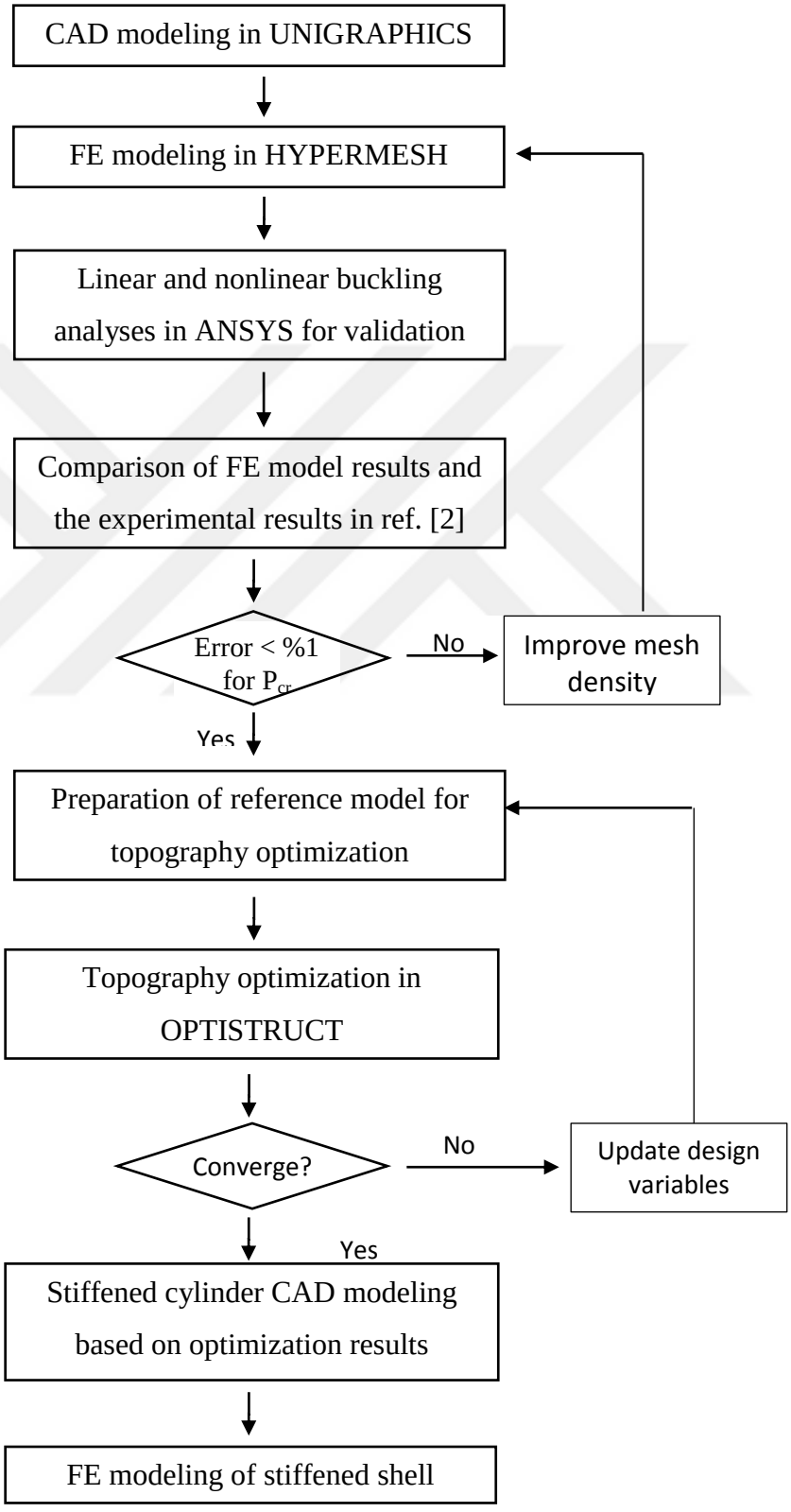
CAD modeling in UNIGRAPHICS
FE modeling in HYPERMESH
Linear and nonlinear buckling analyses in ANSYS for validation
Comparison of FE model results and the experimental results in ref. [2]
Error < %1 for P_{cr}
No
Improve mesh density
Yes
Preparation of reference model for topography optimization
Topography optimization in OPTISTRUCT
Converge?
No
Update design variables
Yes
Stiffened cylinder CAD modeling based on optimization results
FE modeling of stiffened shell

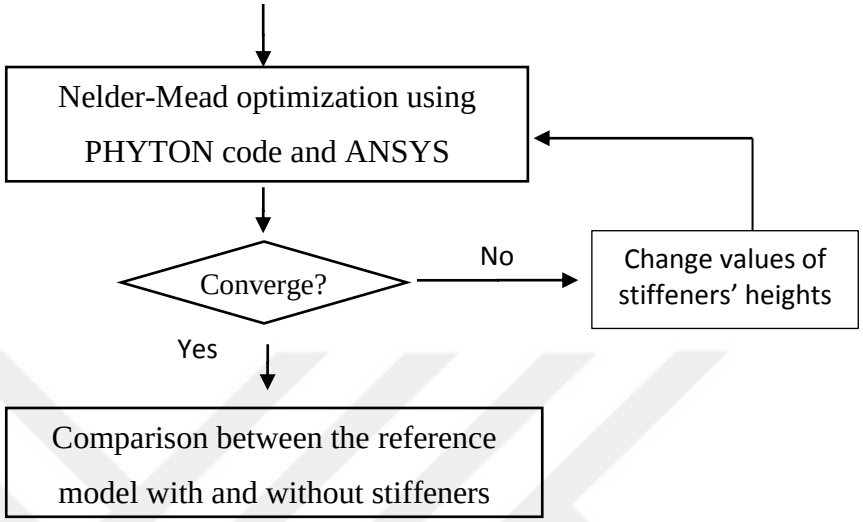

Figure 3.1. Thin-walled cylindrical shell optimization procedure.

4. FE MODEL VALIDATION

4.1. Cylindrical Shell Geometries and Properties for Validation

Three different shell geometries are investigated based on the diameter/length ratio and thicknesses given in reference study [2]. Moderately-thick and thin shells have thicknesses of 0.889 and 0.0889 mm respectively are analyzed for validation. The diameter of all the cylinders is 40 mm. The length of the moderately-thick cylinder is 200 mm. Thin cylinders have two different lengths, 40 mm and 200 mm. The cylinders have a square cutout with dimensions 7.5 mm x 7.5 mm located at the middle. Radius of curvature of the fillets at the corners of the holes is 1.00 mm, which are introduced to reduce stress concentration. Geometrical dimensions are shown in Figure 4.1 and given in Table 4.1. The material of the cylinders was AL 6061-T6 alloy. The engineering stress-strain curve of the material reported by the reference study is used in the FE model. The curve, given in Figure 4.2 was obtained in that study by conducting tension tests on dog-bone specimens according to ASTM B557.The elastic modulus and Poisson's ratio of the material are 68.95 GPa and 0.33, respectively.

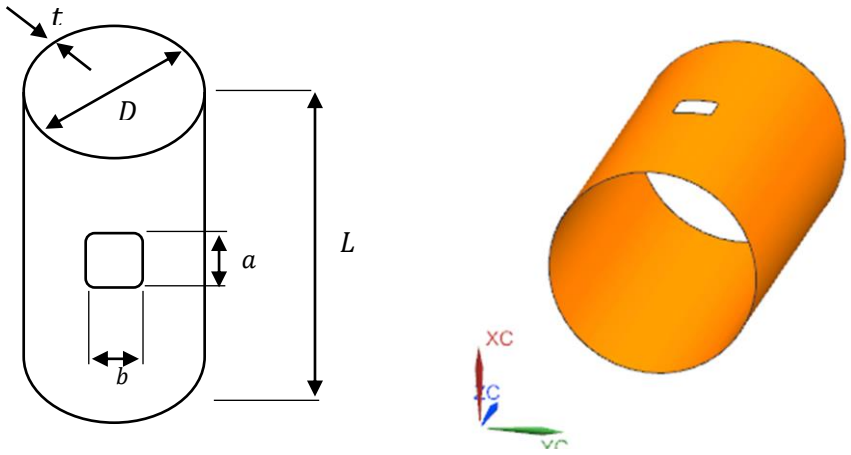

Figure 4.1. The cylindrical shell geometry used to validate the FE model.

Table 4.1. Dimensions of the analyzed shell geometries.

	Diameter (D)	Length (L)	Thickness (t)	(L/D)	(D/t)	a (mm)	b (mm)
Geometry 1	40 mm	200 mm	0.889 mm	5	45	7.5	7.5
Geometry 2	40 mm	80 mm	0.0889 mm	2	450	7.5	7.5
Geometry 3	40 mm	200 mm	0.0889 mm	5	450	7.5	7.5

Multi-linear isotropic hardening material model is used for the nonlinear analyses in ANSYS. In isotropic hardening, the yield surface expands uniformly during plastic flow. This is well suited for simulating large strain deformations. In linear buckling analyses, on the other hand, only elastic modulus and Poisson's ratio are used as material property.

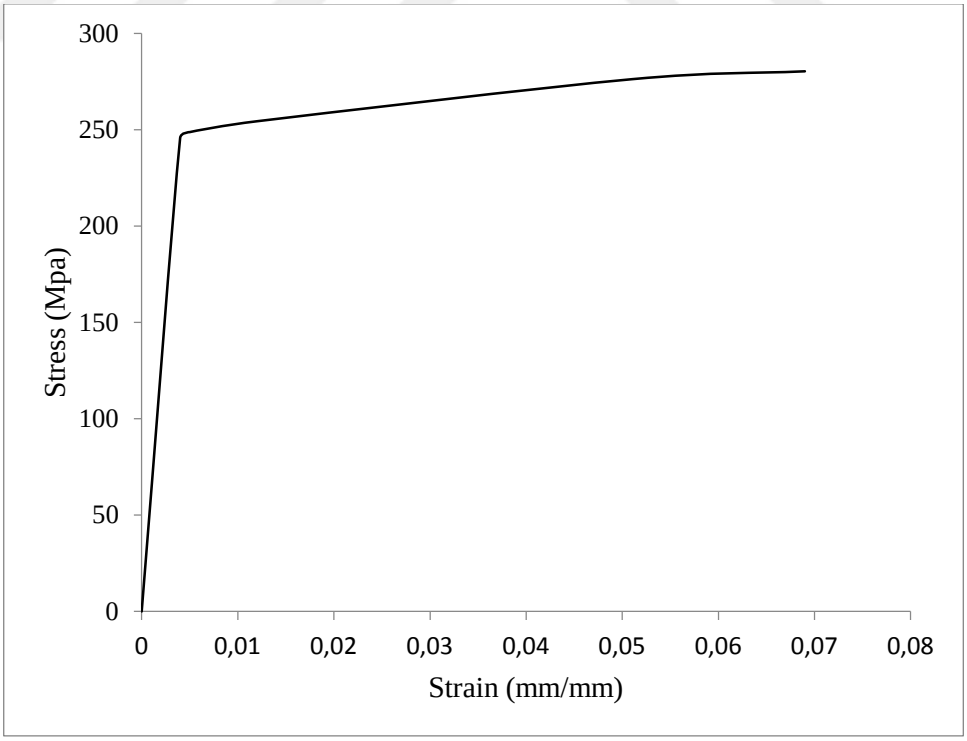

Figure 4.2. Strain-Stress curve of multi-linear isotropic hardening material model in ANSYS.

4.2. Boundary Conditions

Axial force is uniformly applied to the nodes on the top edge of the cylindrical shell and coupled along *z* direction for uniform displacement. Vertical displacement is restrained at the bottom edge and left free at the top end, while lateral displacements in *x* and *y* directions are prevented at both ends. Rotational degrees of freedom in all directions restrained at the bottom and top ends.

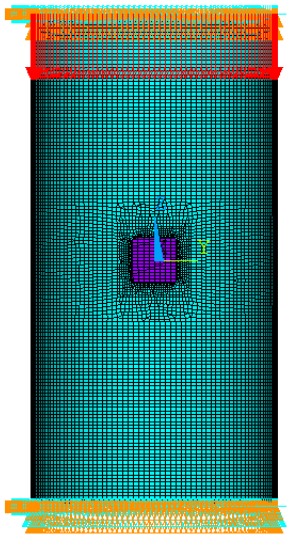

Figure 4.3. FE model with BC's.

4.3. Shell-181 Element

Shell-181 element is used in the FE model, which is very suitable for analyzing thin to moderately-thick shell structures undergoing linear or large-strain nonlinear deformations [19]. It is a four-node element with six degrees of freedom at each node; translations in the *x*, *y*, and *z* directions, and rotations about the *x*, *y*, and *z* axes. Figure 4.4 shows the geometry, node locations, and the element coordinate system for this element. Change in shell thickness is accounted for in nonlinear analyses. The finite element meshes shown in Figure 4.3.

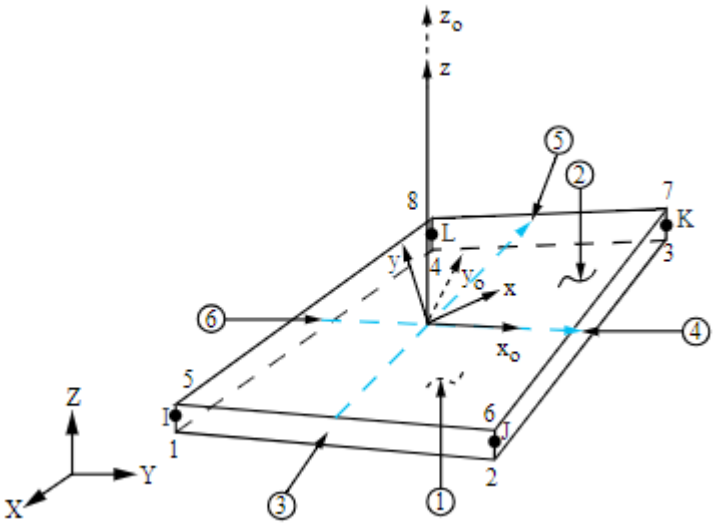

Figure 4.4. Shell-181 element coordinate system and node locations representation [21].

4.4. Linear (Eigenvalue) and Nonlinear (Collapse) Analyses in ANSYS for Validation

Linear FE buckling analysis is performed to predict the theoretical critical buckling load (the first eigenvalue) of the shell structure. The eigenvalue analysis yields the load factor. The critical bucking load is found by multiplying the applied uniform loads on the structure with the calculated load factor. However, the geometrical imperfection due to the cutout leads to nonlinearities that prevent the structure to attain the theoretical buckling strength predicted by the Eigenvalue analysis. Therefore, it is necessary to conduct a nonlinear analysis to accurately predict the non-stable mechanical response of the cylindrical shell with cutout where the basic form of the eigenvalue buckling analysis can be expressed [20] as following

$$[K_e]\{\emptyset_i\} = \lambda_i[K_{\sigma L}]\{\emptyset_i\} \tag{4.1}$$

$[K_e]$ = is the elastic stiffness matrix, $\{\emptyset_i\}$ = is the eigenvector indicating the mode shape, λ_i= is the eigenvalue indicating the load factor, $[K_{\sigma L}]$ is the initial stress matrix.

The eigenvalue solution uses an iterative algorithm that obtains at first the eigenvalue and secondly the displacements that define the corresponding mode shape [20].The eigenvalue represents the ratio between the initially applied load, N_i, and the critical buckling load which is shown as follows:

$$\lambda_i = \frac{p_{cr}}{N_i} \tag{4.2}$$

Therefore, it is often said that the eigenvalue is like a safety factor for the structure against buckling. On one hand, an eigenvalue less than 1.0 indicates that a structure buckles under the applied loads. On the other hand, an eigenvalue greater than 1.0 indicates that the structure does not buckle.

In order to correctly determine locally unstable response, a nonlinear buckling analysis is performed. It is a static structural analysis with large deflection effects of finite elements being turned on. A gradually increasing load is applied to seek the load level at which the structure becomes unstable. The nonlinear analysis takes into consideration both geometric and material nonlinearities. Nonlinear analyses for each of the three geometries are conducted using arc-length method as in the reference study [2] to obtain the post-buckling behavior. An application of the arc-length method involves the tracing of a complex path in the load-displacement response into the both buckling and post buckling region.

4.5. Sensitivity Study for Mesh Sizing

In order to determine an appropriate mesh size, geometry 2 is chosen and several linear buckling analyses are conducted with different mesh sizes. The results are given in Table 4.2. Nonlinear analyses also performed for last three mesh sizing and results are shown in Table 4.3. Considering the convergence of solution in terms of buckling load, 0.5 mm (252 x 140) is used in both linear and nonlinear analyses.

Table 4.2. The values for the critical buckling load calculated by the linear analysis for different mesh sizes (geometry 2).

Avg. mesh size	Applied load (N)	Buckling load factor	Critical buckling load (N)
3 mm (40 x 30)	40	12.354	494.1
2 mm (60 x 40)	60	6.1926	371.5
1 mm (126 x 80)	126	2.6698	336.4
.875 mm (144 x 80)	144	2.2992	331.1
.675 mm (144 x 140)	144	2.2378	328.1
.500 mm (252 x 140)	252	1.2788	328.3
.375 mm (300 x 200)	300	1.0743	328.3

Table 4.3. The values for the critical buckling load calculated by the nonlinear analysis for different mesh sizes (geometry 2).

Avg. mesh size	Critical buckling load (N)
.675 mm (144 x 140)	732.9
.500 mm (252 x 140)	734.7
.375 mm (300 x 200)	735.2

4.6. Validation of the Finite Element Model

Nonlinear analyses are carried out for all three geometries and compared with the experimental and numerical results in the reference study [2]; but linear buckling analyses are only conducted for thin-walled cylinder (geometries 2 and 3) and compared with the linear analysis results in the previous study [2] because of the absence of experimental results for thin shells. For moderately thick shells, reference load, N_{ref} is defined as 245 N/mm by multiplying the yielding strength with thickness as in the reference study and the applied load can be found 30787 N by multiplying N_{ref} with the perimeter. The total axial load N is divided by N_{ref} for normalization purpose, similarly deflection towards z axis (end-shortening), δ, is divided by cylinder length.

4.5.1. Moderately Thick Cylinder

Numerical results obtained for moderately thick cylinder (geometry 1 in Table 4.1) via nonlinear FE analysis are shown in Figure 4.5. Numerical and experimental results reported by the reference study [2] for the same geometry are given in Figure 4.6. The normalized load – deflection curve obtained by the present FE model is almost the same as the numerically obtained one in the reference study [2] as shown in Figure 4.5. The differences between the numerically obtained curves may be due to the differences in the mesh densities. Von Misses stress contour plots of the present study are compared with the similar plots of the reference study as well as the pictures from experiments corresponding to three (A, B, C) levels shown in Figure 4.7. which show from left to right, von Misses stress plot and picture from the experiments of the reference study, and von Misses stress plot of the present study for each level shown on load - end shortening curve of present study for geometry 1 ($L=5D$, D/t = 45).

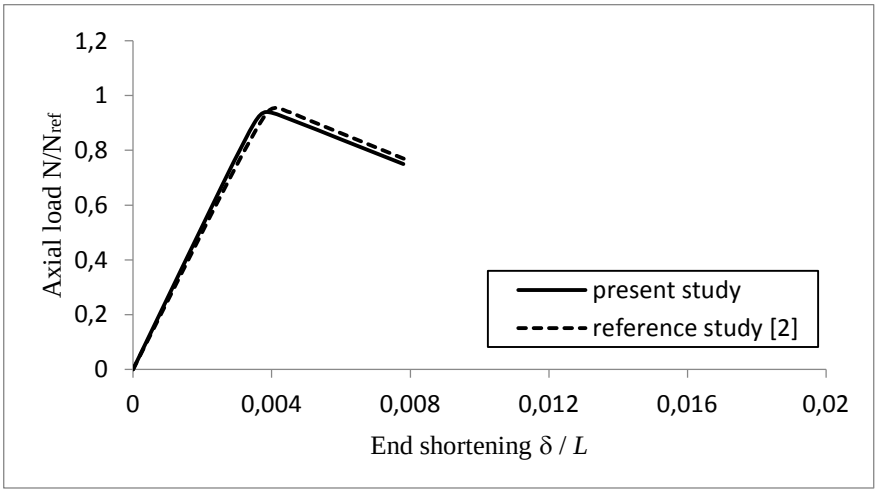

Figure 4.5. Comparison of normalized end shortening - load curves obtained by FE analysis carried out in the present study and the reference study [2] (geometry 1).

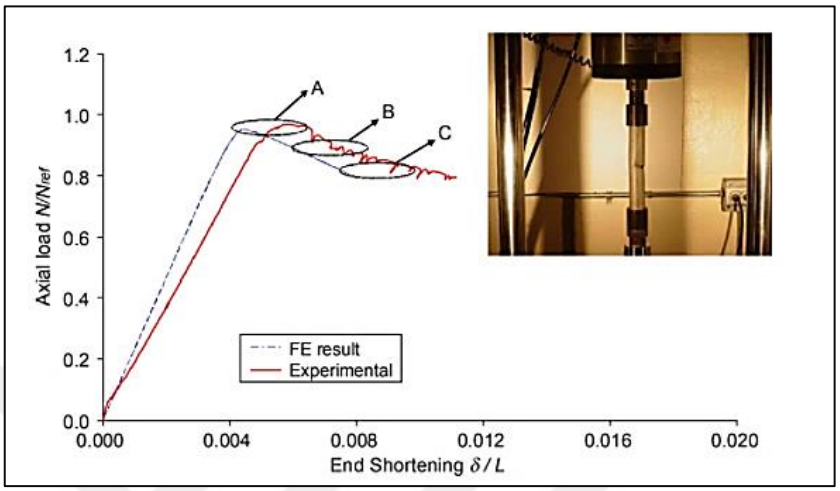

Figure 4.6. The reference study [2] (geometry 1).

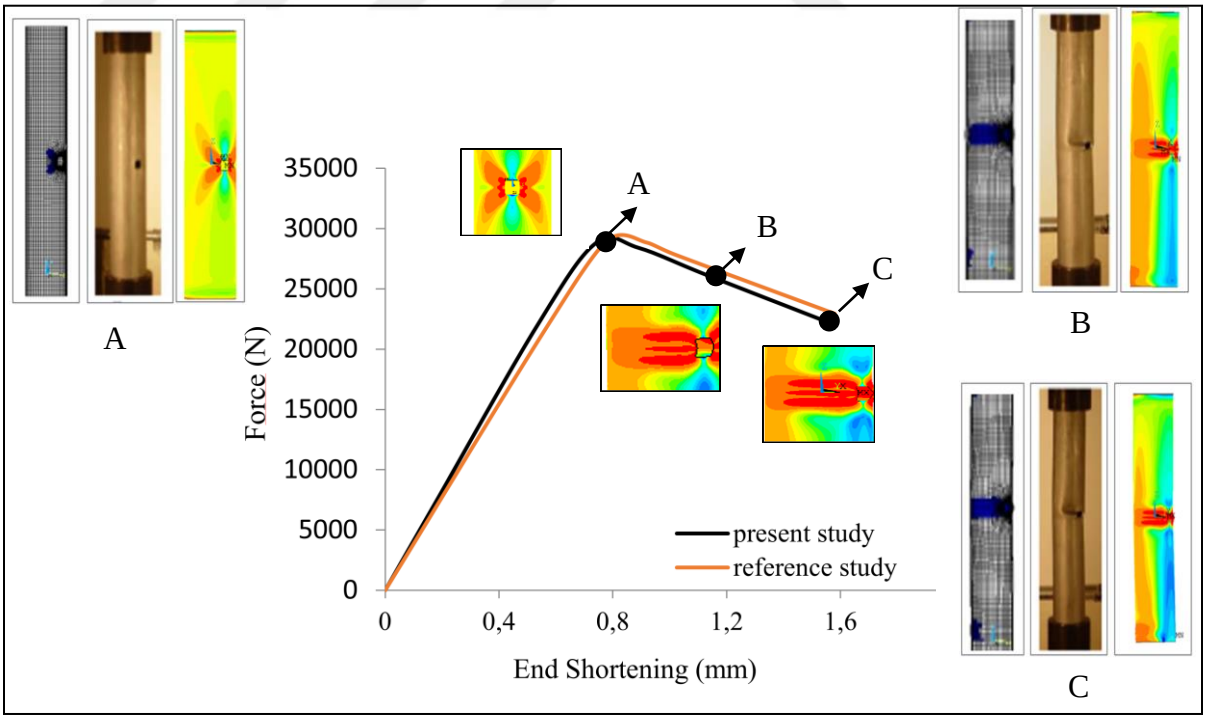

Figure 4.7. Comparison of the experimental and numerical results of the reference study [2] and the numerical results of present study, which are shown by the colored contour plots of equivalent stress (geometry 1).

4.5.2. Thin-Walled Cylinder

For thin cylindrical shells both nonlinear and linear buckling analyses are performed for geometry 2 and geometry 3 with *L/D* ratio being equal to 2 and 5, respectively. Normalized load versus end shortening curves are generated from nonlinear analyses till the first peak buckling strength for both geometries as shown in Figure 4.8 and Figure 4.9. It is observed that local buckling occurs before section yielding. Post buckling behavior is not as smooth as moderately thick shell.

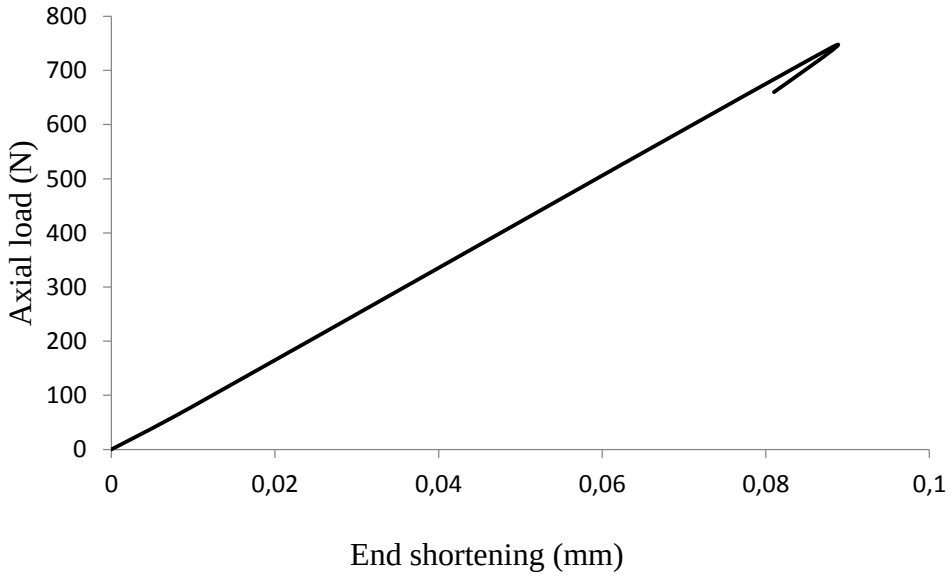

Figure 4.8. Normalized load vs end shortening plot obtained by the nonlinear analysis for $L=2D$ and $D/t = 450$ (geometry 2).

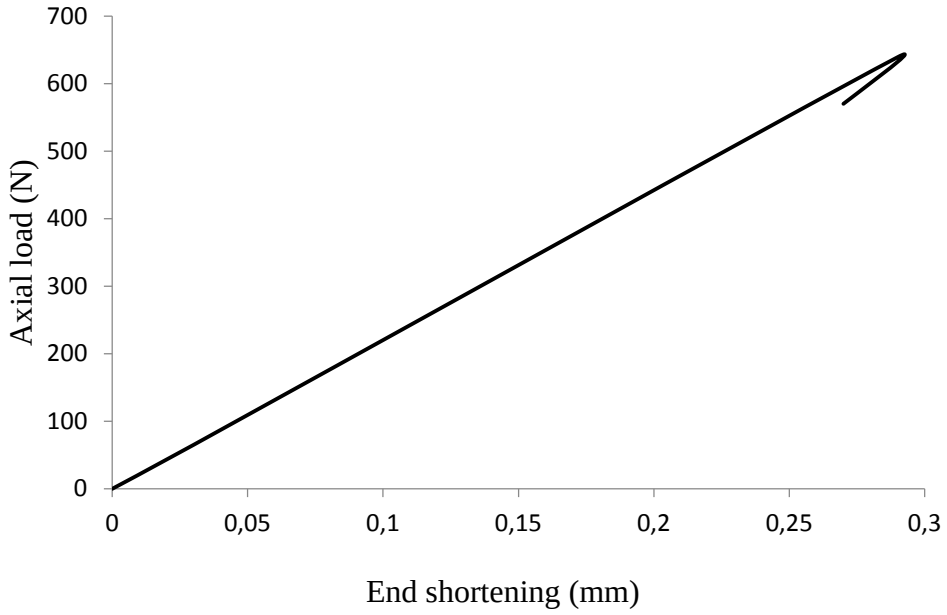

Figure 4.9. Normalized load vs end shortening plot obtained by the nonlinear analysis for L=5D and D/t = 450 (geometry 3).

Linear and nonlinear buckling analyses are performed for thin cylinders and the results of the present study together with the results of the reference study are tabulated in Table 4.3. The numerical results compare well with that of the reference study. The critical buckling load predicted by the nonlinear analysis is about two times larger than that of the linear eigenvalue buckling analysis. Since the linear analysis result does not correlate with experiment, it will not be used in the optimization process where stiffener height is determined.

Table 4.4. Buckling loads (N) comparison, present vs. ref. study for thin shells (D/t = 450).

	L = 2D (geometry 2)	L=5D (geometry 3)
Linear analysis	328.2	293.1
Linear analysis [2]	333.4	296.9
Nonlinear analysis	734.7	638.9
Nonlinear analysis [2]	740.1	642.2

5. OPTIMIZATION STUDIES AND RESULTS

5.1. The Reference Cylindrical Shell

OPTISTRUCT solver is used for topography optimization. The dimensions of the reference cylinder are taken the same as that of the moderately thick cylinders with a square cutout tested in the previous study [2], but the optimized cylinder contains two square cutouts considering the similarity of the exhaust case in Figure 1.1 (b). Moderately thick shell is studied smoother post buckling behavior compared to cylindrical shell. Both linear and nonlinear analyses are performed in ANSYS but since it shown in validation section, nonlinear analysis is necessary to simulate reality with more accuracy.

5.1.1. Cylindrical Shell Geometry

In the reference geometry, diameter, D, length, L, and thickness, t, are chosen the same as the one used in the validation study, however, the cutout size is increased from 7.5 mm x 7.5 mm to 10 mm x 10 mm. All dimensional information is given in Table 5.1.

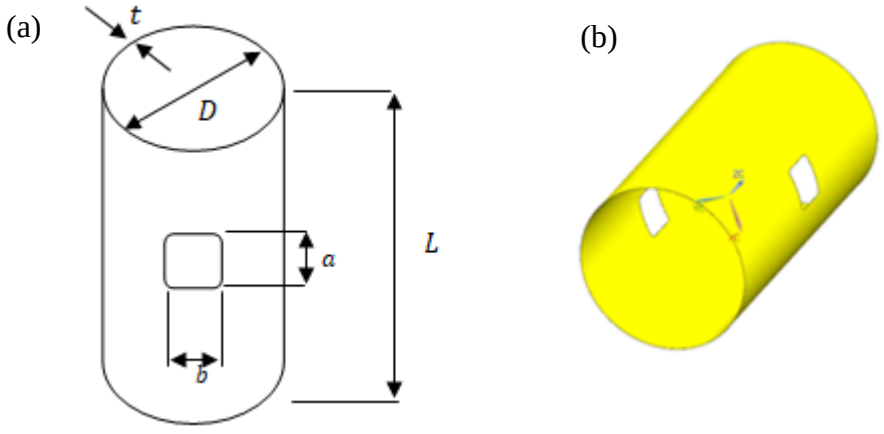

Figure 5.1. (a) Schema for the reference geometry, (b) its CAD model.

Table 5.1. Dimensions of the reference shell geometry for optimization

	Diameter (D) (mm)	Length (L) (mm)	Thickness (t) (mm)	L/D	D/t	a (mm)	b (mm)	Number of holes
Ref. Geometry	40	80	0.889	2	45	10	10	2

5.1.2. Finite Element Modeling

The FE model for the reference geometry is developed in HYPERMESH and meshed using the same average element size, 0.500 mm, as determined in the model validation study. The meshed geometry is shown in Figure 5.2. It is imported to ANSYS to carry out linear and nonlinear analyses as. The boundary conditions are the same as in the validation study: The nodes at the bottom edge are fixed; only vertical displacement is allowed at the top edge. Rotations are restricted for both the top and bottom edges. Pressure is applied to the all nodes at the top edge uniformly. Multi-linear kinematic hardening model is used with the same strain-stress curve (Figure 4.2) used for validation. Nonlinear analyses are performed using the arc-length method to observe the post-buckling behavior. Besides, in the linear isotropic material model, the elastic modulus and Poisson's ratio are chosen as 68.948 and 0.33, respectively, which correspond to the properties of Aluminum used in the previous study [2].

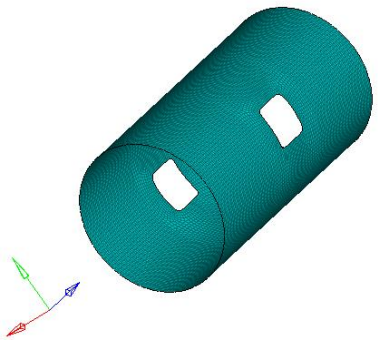

Figure 5.2. Meshed geometry in HYPERMESH

5.1.3. Results for the Reference Geometry

Nonlinear large strain displacement analysis is conducted for the reference shell with two symmetrical cutouts at the middle. End shortening versus load curve is obtained from the results for the vertical displacement at the top edge and the reaction forces in the *z* direction at the bottom edge. The results show that the maximum buckling load capacity of the reference geometry is 22051 N corresponding to point B in Figure 5.3. Von Misses and displacement plots for points A, B and C are also shown in the figure. It can be seen that stress accumulates in the same region as in the cylinder used in the validation study. The maximum displacement and stress occur around the cutout. Gross bucking of the cylinder starts at the middle region. Buckling occurs more uniformly due to the symmetrically placed two cutouts.

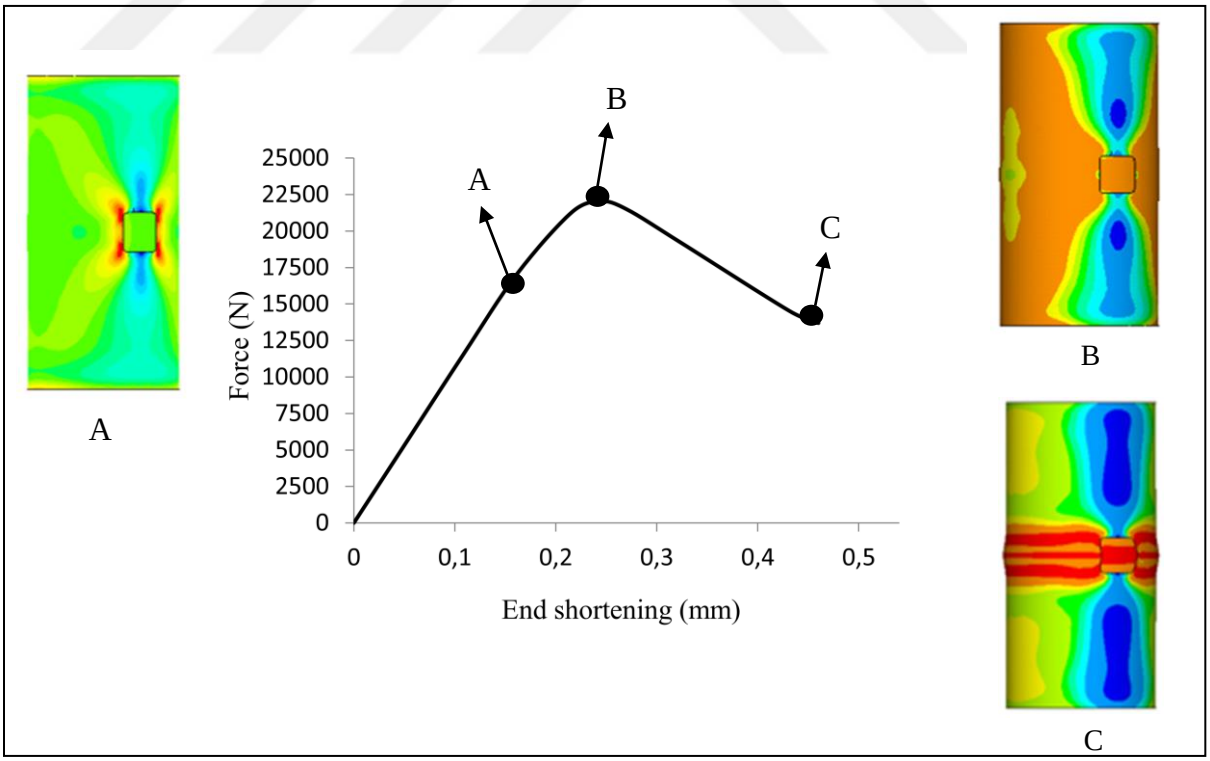

Figure 5.3. End shortening versus load curve for the reference geometry and von Misses stress plot (left) and the total displacement plot (right) corresponding to A, B, C points on the curve, D/t= 45, L=2D

Additionally, linear analyses are performed in both OPTISTRUCT and ANSYS. Both results are very similar to each other as expected. The results in terms of buckling load capacity, results are presented in the form of buckling load factor, which is defined in Equation 4.2.

Table 5.2. Linear buckling analyses results

	Initially applied load (N)	Buckling load factor	Critical buckling load (N)
OPTISTRUCT	252	304.2	76633
ANSYS	252	304.9	76834

The conclusion of this comparison shown in Table 5.2 is that there would be no difference if topography optimization were performed using ANSYS solver instead of OPTISTRUCT for linear buckling sub-case.

Besides, comparing linear analysis results with the nonlinear analysis, linear analysis predicts around 3.5 times larger buckling load.

5.2. First Level of Optimization (Topography Optimization)

Topography is a type of optimization is aimed to maximize stiffness of components creating a pattern of shape variable-based reinforcement within the design domain along the shell surface. Topography is an advance form of shape optimization and it is different from topology optimization, that is, topography optimization utilizes shape variables on the shell surface instead of material distribution of variables. In this study, the design domains defined as the entire outer surface of the structure except small strips of one element size at the top and bottom as well as around the cutouts for convergence easiness which shown with orange colored elements in Figure 5.4. Considering shell thickness remains the same during the optimization, no stiffener is generated in these one element size regions.

Topography optimization is conducted for the reference shell geometry to obtain the optimum stiffener configuration on the shell surface for maximum buckling load capacity. Optimization is performed in OPTISRUCT, which evaluates the bucking capacity based on the linear analysis. OPTISTRUCT automatically selects most proper optimization algorithm within the several options such as optimally criteria method, convex approximation method and method of feasible directions. Optimally criteria method is used for the present design problem. Stiffener angle, width and height are used as design variables as shown in Figure 5.5.

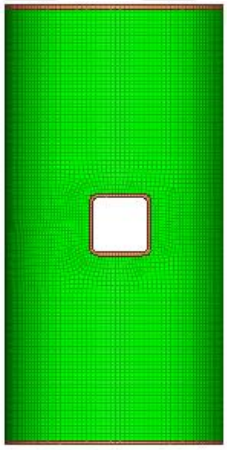

Figure 5.4. The meshed geometry with green colored elements representing the design domain and orange colored elements non-design domain for the topography optimization.

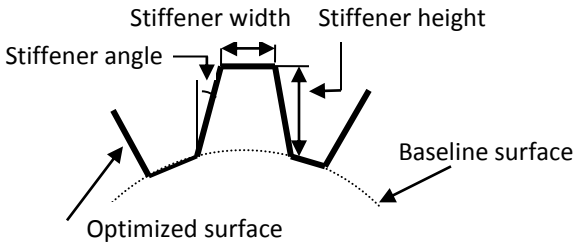

Figure 5.5. Schematic representation of the design constraints on stiffener geometry

5.2.1. Design Constraints

During stiffener optimization, the slope of the stiffeners with respect to base line and their height and width can be varied. Upper limits may need to be imposed for these variables in order to prevent the optimization algorithm from assigning inappropriate values for them. These constraints are schematically shown in Figure 5.5. A height constraint is not imposed during the topography optimization, because Nelder-Mead local search optimization is subsequently conducted to determine the optimum stiffener height and shell thickness. Topology optimization is conducted to find the optimum stiffener configuration on the shell surface not to find the optimum thickness and different than Nelder-Mead optimization, shell thickness is not included optimization process. The height constraint does not significantly affect the optimum stiffener configuration changing as shown in Figure 5.6; it only affects the relative stiffener height. Thus, 1.0 mm is used as the upper limit and lower limit is set to be equal to shell thickness on stiffener height for topography optimization.

$$0 \leq S_H \leq 1.00 \tag{5.1}$$

In order to choose a suitable value for the width constraint, a sensitivity study is conducted to see its effect on the optimum stiffener configuration; several values for the width constraints are as lower limit tried keeping the rest of the design constraints the same. The results show that the resulting optimum stiffener configurations are very similar as shown in Figure 5.7. Because there is no gap limit for the stiffeners thus, program may locate stiffeners adjacent to each other thus regardless of the width limit software adjacent enough number of stiffeners and end up with required width. In addition to this, it is not allowed to set a value for minimum width lower than a finite element width. In this case, min limit cannot be lower than 0.5 mm but exactly 0.5 mm limit causes an error during the optimization process. Due to the fact that 1 mm is also chosen for minimum width constraint limit.

$$1.00 \leq S_W \tag{5.2}$$

The stiffener angle is not taken as a variable a constant value of 90 degrees is chosen; thus the stiffeners are implemented on shell surface towards to normal direction. It should be noted that in order to reduce stress concentrations, fillets need to be introduced between the stiffeners and the shell.

In order to prevent the algorithm to generate stiffeners on all over the shell surface, i.e. increasing thickness uniformly, an upper limit is set for the maximum volume of stiffeners that can be generated on the shell surface. Otherwise, the algorithm would set the stiffener height equal to its upper bound, which is 1.0 mm, all over the shell surface to maximize the buckling strength. In this study, the upper limit for the volume fraction of stiffeners is chosen to be 0.4. Thus, the volume of stiffeners does not exceed the 40% of design region volume. The lower limit is taken as zero.

$$V_S \leq 0.4V_D \tag{5.3}$$

5.2.2. Objective Function

The objective function to be maximized is the bucking factor. This means that maximizing the buckling strength of the structure is the aim of the optimization. The optimization problem can be expressed as

$$\text{Maximize:} \quad f = P_{cr} \tag{5.4}$$

$$\text{Subjected to:} \quad 0 \leq S_H \leq 1.00 \tag{5.5}$$

$$1.00 \leq S_W \tag{5.6}$$

$$V_S \leq 0.4V_D \tag{5.7}$$

5.2.3. Mesh Size, Properties and Boundary Conditions

The same mesh size, boundary condition and material properties are used for the topography optimization as in the reference shell structure. Linear isotropic material is defined with elastic modulus and Poisson's ratio being equal to 68.948 and 0.33, respectively.

5.2.4. First Level Optimization Results

OPTISTRUCT is used as solver and the results are viewed in HYPERVIEW. For better understanding of the results, contour shows stiffener height representing by different colors is divided based on the various stiffener heights and the same plots in Figure 5.6. and 5.7. show the surface shape changes after the topography optimization. The most critical regions, where local buckling may occur, are shown with red color, where stiffener height is close to its upper limit 1.0 mm. One critical region is the sides of the cutouts and the other is the top and bottom ends, which are called "elephant food location" in the literature. Stiffeners can be grouped to their heights in three main groups having 0.3, 0.4, and 1 mm heights as shown in Figure 5.8.

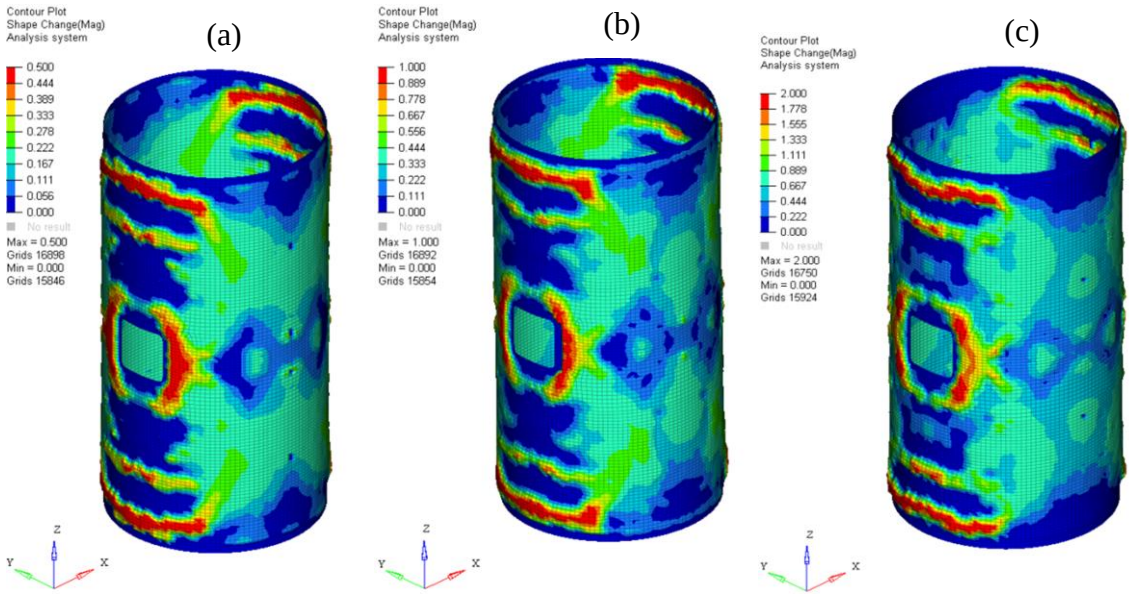

Figure 5.6. Topography optimization results obtained for different upper limits for stiffener height (a) 0.500 mm, (b) 1.00 mm, (c) 2.00 mm.

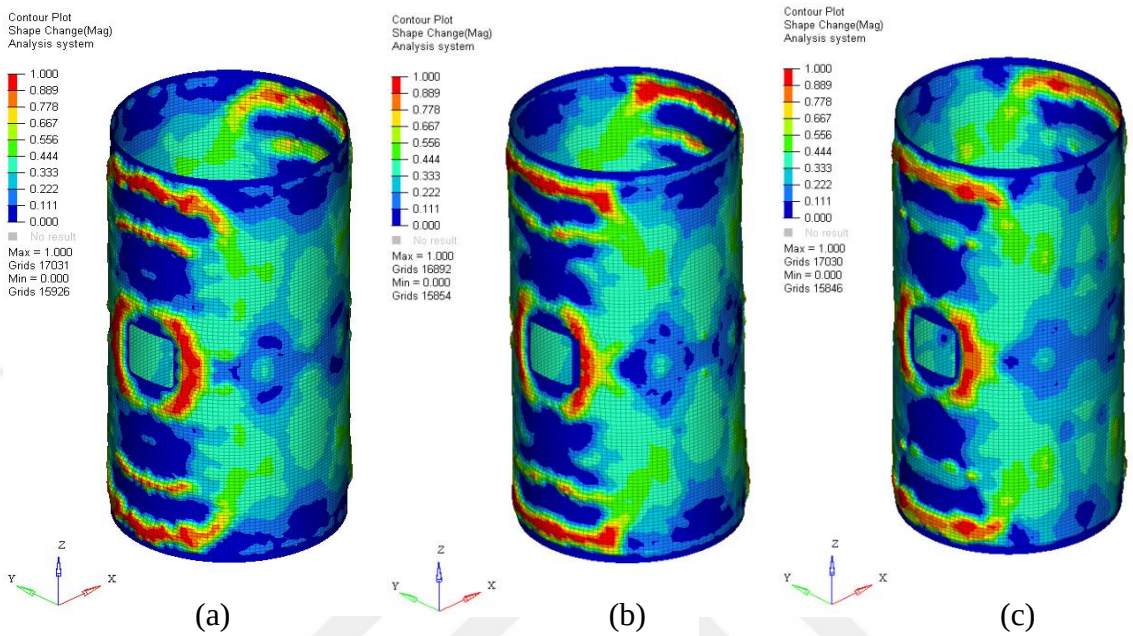

Figure 5.7. Topography optimization results obtained for different lower limits on stiffener width, (a) 0.625 mm, (b) 1.00 mm, (c) 2.00 mm.

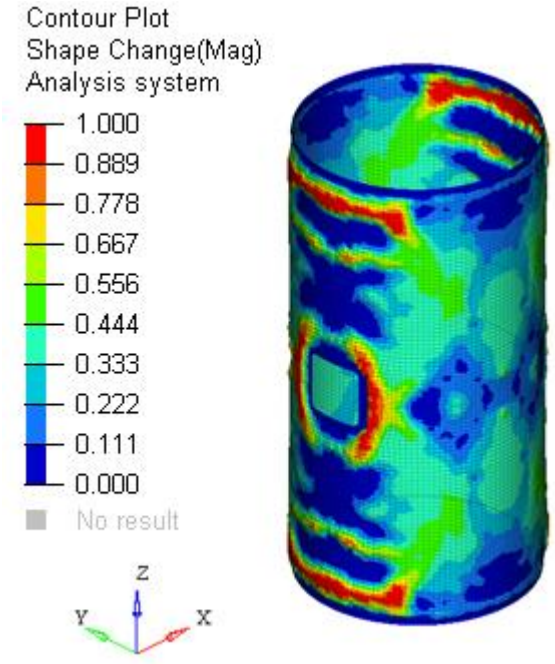

5.8. Contour plot for optimum stiffener configuration showing relative stiffener height

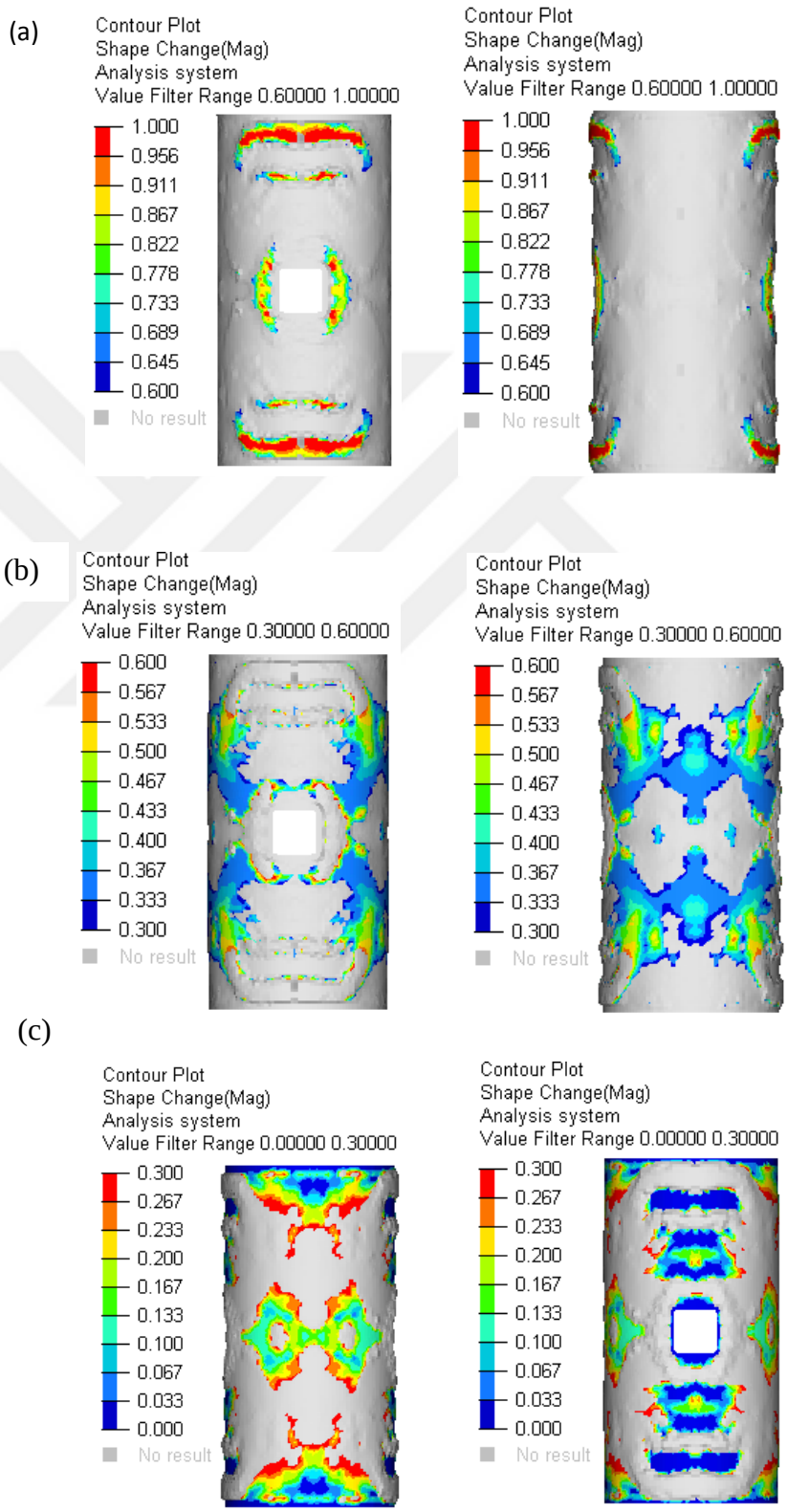

Figure 5.9. Contour plots for different ranges of height in mm (a) 1-0.6, (b) 0.6-0.3, (c) 0.3-0.

5.3. Second Level of Optimization (Stiffener Height Optimization)

5.3.1. Stiffener Configuration

Three different stiffener patterns can be distinguished in different regions of the shell surface from the contour plots of the topography optimization as shown in Figures 5.10 and 5.11. The orange-colored stiffener corresponds to 0.6-1.00 mm range of thickness in the contour plot given in Figure 5.9 (a). They provide the main support around the cutouts and elephant foot locations in the structure, which are the weakest parts of the structure against buckling as shown in Figure 5.12. Thus, 1 mm-height stiffeners are used in these locations. The widths of the stiffeners are directly obtained from the topography optimization results; accordingly, the cut out and elephant foot locations have wider, 2 mm, stiffeners. Although there is no connection is observed between cutouts and elephant foot locations in 0.6-1.00 mm plot, 1 mm- height stiffeners are placed towards 45° for the connection of those two critical locations in order to provide extra rigidity. For the range of 0.3-0.6 mm height, the topography optimization algorithm creates regions with uniform height. For those regions, rather than thickening the entire area, stiffeners are generated to form small stiffened square areas, which is similar to the pattern used in a previous study [10]. Thus orthogrid pattern with stiffeners having 0.3 mm-height and 0.3 mm-width is issued to avoid weight increase for locations where a large area needs to be thickened according to the results as shown in Figure 5.9 (c) and the blue-colored stiffeners with 0.4 mm height and 1 mm-width are used as dividers of those regions. The range of 0-0.3 mm height should be place with smaller stiffeners or left empty to gain weight.

While determining the final stiffener configuration, other studies are also considered as shown in Figure 5.12. The reason of the configuration found by OPTISTRUCT is not directly used is because OPTISTRUCT uses linear analysis and this does not yield accurate results. As it is mentioned in section 5.1.3, comparing linear analysis results with the nonlinear analysis, linear analysis predicts around 3.5 times larger buckling load thus the stiffener configuration optimized by the software cannot be considered as optimum with confidence.

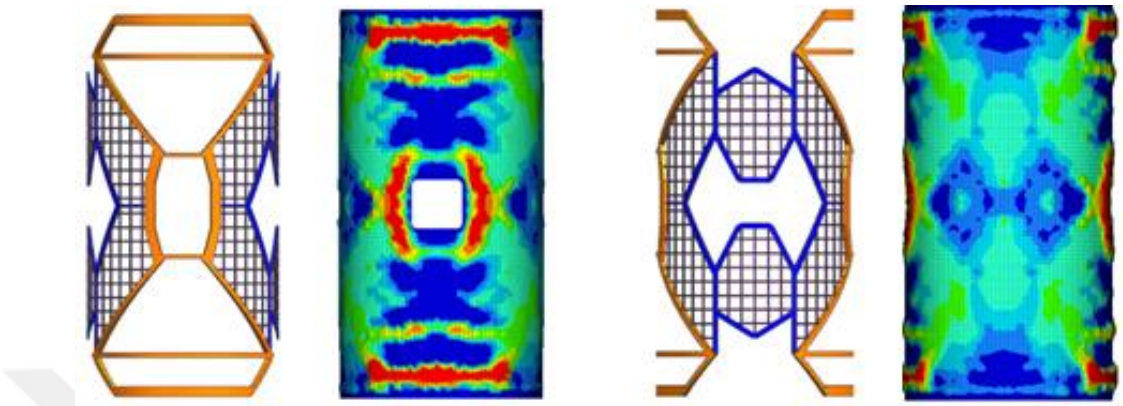

(a) (b)

Figure 5.10. (a) Front view of stiffener CAD model and topography optimization result, (b) rear view of the stiffener CAD model and the topography optimization result.

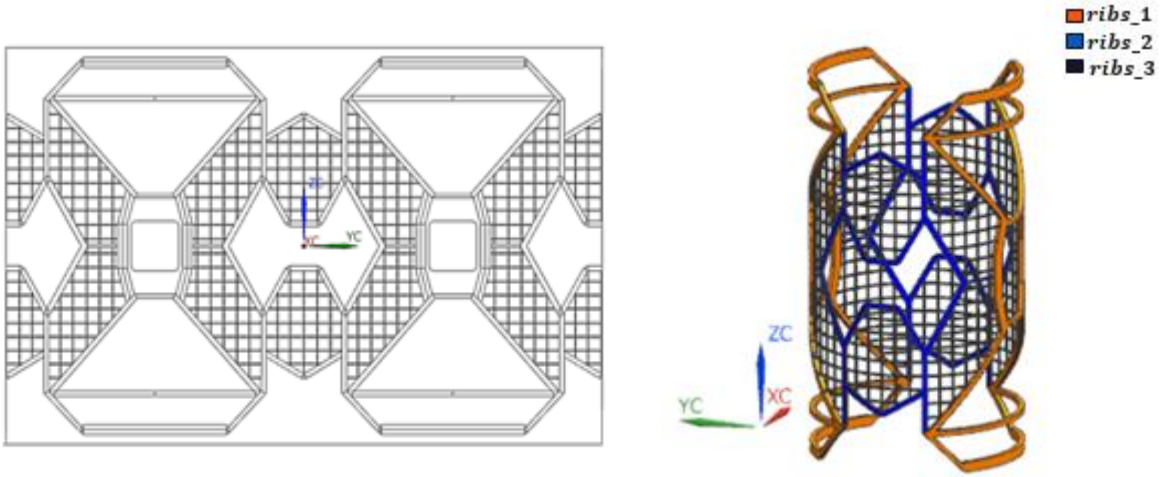

(a) (b)

Figure 5.11. (a) 2D stiffener configuration, (b) 3D CAD model of the stiffeners.

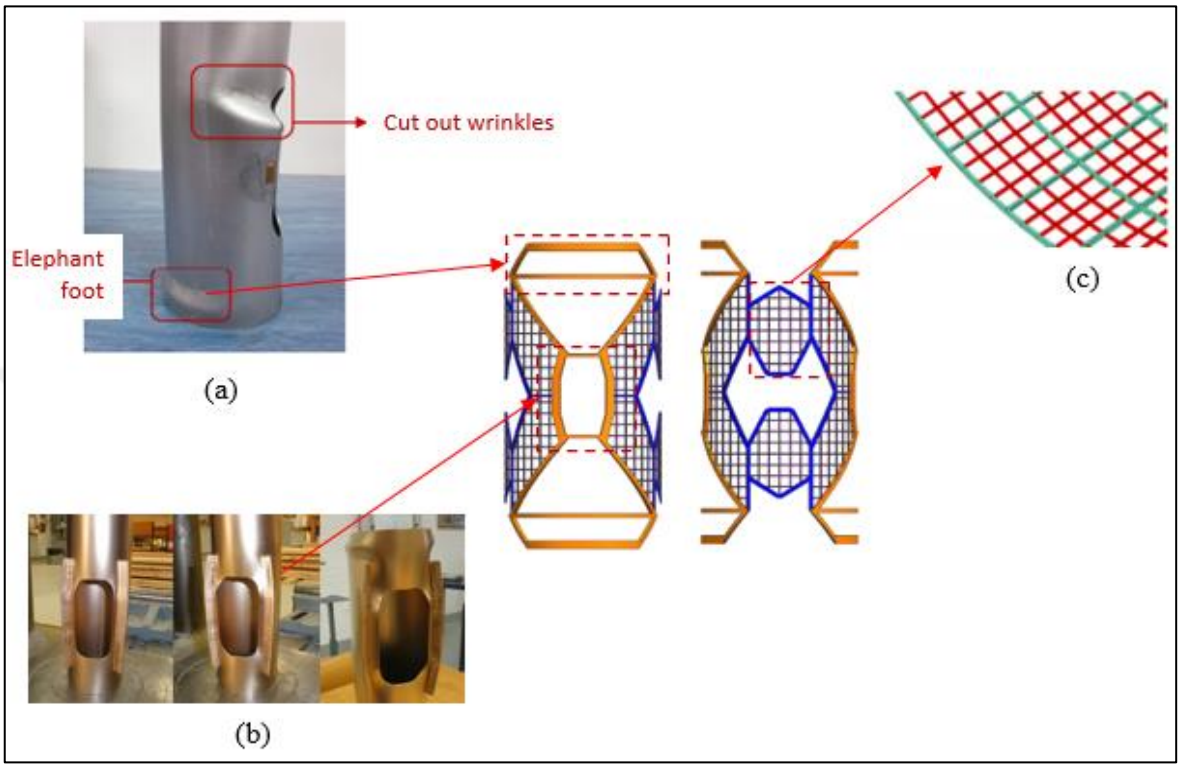

Figure 5.12. The pictures in (a) and (b) show examples of stiffener configurations in the literature [14], The picture in (c) shows the stiffener configuration on cylindrical shell in reference [10].

5.3.2. Stiffener Dimensions and FE modeling

Stiffeners are modeled using shell-181 type of element in ANSYS as integral parts of the cylindrical shell instead of defining bounded contact with stiffeners which is used for welded stiffeners. The heights of the stiffeners are defined as shell thickness; this means the thickness of a finite element is the sum of the shell thickness and the stiffener height at its location. The stiffener material is defined the same as that of the shell. 0.3 mm mesh size is used for thin stiffeners and 0.5 mm issued the rest of the geometry. The meshed stiffened geometry in ANSYS is shown in Figure 5.13.

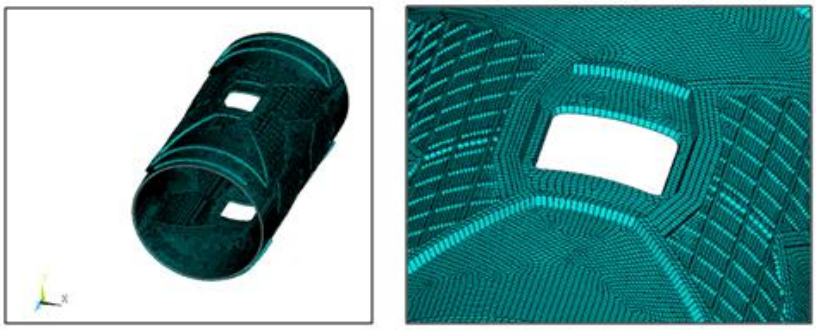

Figure 5.13. The meshed model of the stiffened cylindrical shell in ANSYS

5.4. Nelder-Mead Optimization

In the second level of optimization, the aim is to obtain the optimum values of the shell thickness and the stiffener heights based on the stiffener topography optimized in the first level so that the load-carrying capacity of the structure will be maximum without increase in mass. Nelder-Mead local search algorithm is used to find the optimum design. The buckling load is extracted from the result of nonlinear finite element analysis for each configuration. Nelder-Mead is integrated with ANSYS via PHYTON code that generates a code written in ANSYS Parametric Design Language (APDL) to update the FE model and run nonlinear analysis for each new configuration generated by Nelder-Mead algorithm.

5.4.1. Objective Function

The objective of the optimization is to maximize the critical buckling load of the structure. Because the optimization problems are posed as minimization problems in the standard implementation of optimization methods, the objective function is taken as negative of buckling load. This is mathematically equivalent to the problem of maximizing the buckling resistance of the structure. In order to evaluate the value of the objective function, nonlinear bucking analyses are conducted using ANSYS solver. Structural analyses are performed and the optimization algorithm is implemented by developing a PYTHON code.

5.4.2. Design Variables

The heights of the three stiffeners shown in Figure 5.11 and the shell thickness are defined as optimization variables, but they are not independent. As the heights of the stiffeners are changed by the algorithm in each iteration, the shell thickness is recalculated to keep the weight the same as the unstiffened shell. The problem is therefore a three-dimensional problem for Nelder-Mead Simplex Method. The height of a stiffener is defined as the distance from the bottom shell surface to the top of the stiffener in the second level optimization as shown in Figure 5.14. Considering that Nelder-Mead is a local search algorithm and its computational is high, initial values for the design variables are chosen according to the topography optimization results in order not to start far from their expected optimum values.

5.4.3. Design Constraints

No design constraints are defined for the design variables in terms of upper or lower bounds besides the mass constraint for the stiffened cylinder. Since the stiffener configuration is not changed in the second level of optimization, the surface area of each group of stiffener remains the same while the stiffener heights are varied. Whenever a new configuration is generated by Nelder-Mead algorithm, surface areas of the stiffeners are multiplied by their heights to obtain the volume of the stiffeners. This is then subtracted from the total volume of the unstiffened geometry. The resulting value is divided to the rest of the shell surface area to find shell thickness. Therefore, mass constraint is imposed by eliminating dependent variable.

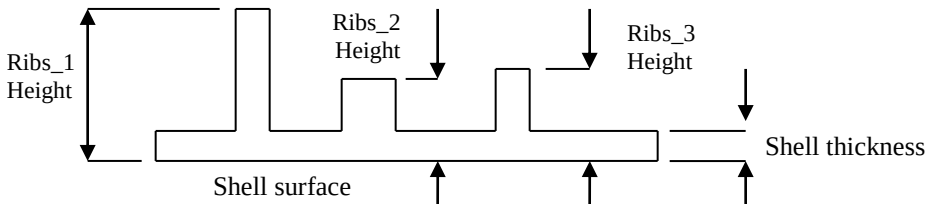

Figure 5.14. Schematic representation of the heights of the stiffeners as they are defined in the optimization code and the shell thickness.

5.4.4. Optimization Code

The optimization code is written in PHYTON to implement Nelder-Mead Algorithm and carry out nonlinear buckling analyses in ANSYS. The optimization procedure is given in Figure 5.15.

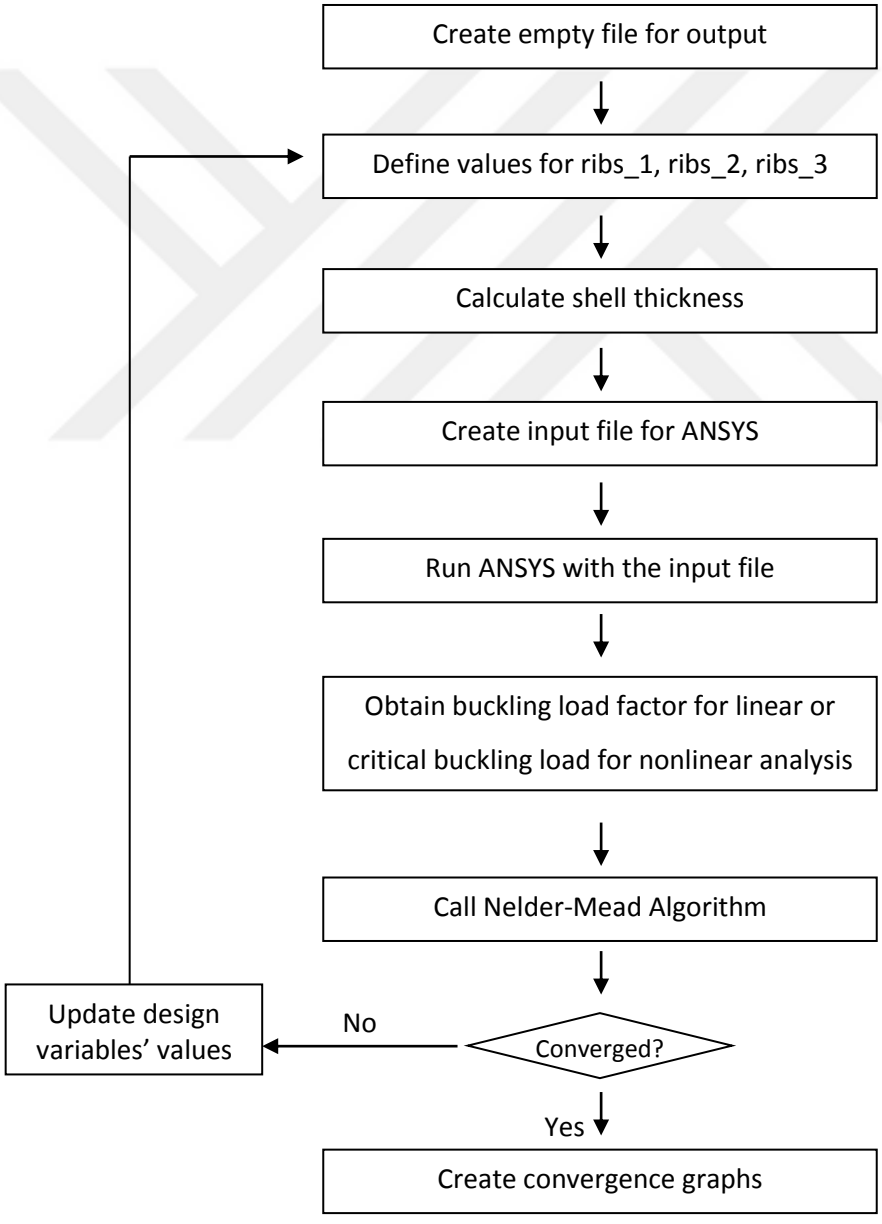

Figure 5.15. The Nelder-Mead optimization procedure

The optimization process starts by assigning initial values for the design variables, then the shell thickness is calculated based on the surface area of each stiffener as explained in Section 5.4.3, after that an input code is generated to update the geometry and run the FE model in ANSYS. After the buckling analysis is carried out in ANSYS, the critical buckling load is extracted and written to an output file. According to the decision criteria of Nelder-Mead algorithm, a new configuration is generated based on the analysis results. The iterations are continued until convergence occurs and the optimum sets of values are found for the design variables that makes the buckling load highest.

5.4.5. Second-Level Optimization Results

Local search optimization is performed via Nelder-Mead method. Initial points of the design variables are chosen according to the topography optimization results. Hence, starting values of 2.00 mm, 1.50 mm and 1.50 mm are used for the heights of ribs_1, ribs_2 and ribs_3 in the optimization process. Nelder-Mead algorithm requires $n + 1$ number of starting points. Other starting points are defined by reducing 10% from the initial value of one of the design variables and keeping the rest of them the same. Repeating this process for other variables, three starting points are obtained other than the initially chosen one. The iteration values of the design variables in terms of stiffener thickness and the corresponding shell thickness are given in Figure 5.16. The results show that ribs_1, which provides support around the cutouts and elephant-foot locations, should be the only group of stiffeners on the shell surface. As indicated in Figure 5.14, the stiffener height also includes the shell thickness. It can be observed from the Figure 5.16 that the converged values of ribs_2 and ribs_3 are very close to the shell thickness, which means they actually do not make a significant contribution on the buckling strength of the structure compared to ribs_1 (main supports); thus those two stiffener groups located on lateral surface of shell should be eliminated from the final stiffener configuration. Nonlinear buckling analysis is conducted in ANSYS to find the value of the objective function, which is the critical buckling load in each iteration. Figure 5.17 shows the iteration values of the critical buckling load versus number of iterations. Results show that sometimes stiffener thickness takes a value lower than the shell thickness, which introduces

another geometrical imperfection and it causes considerable decrease of buckling load-carrying capacity of the structure.

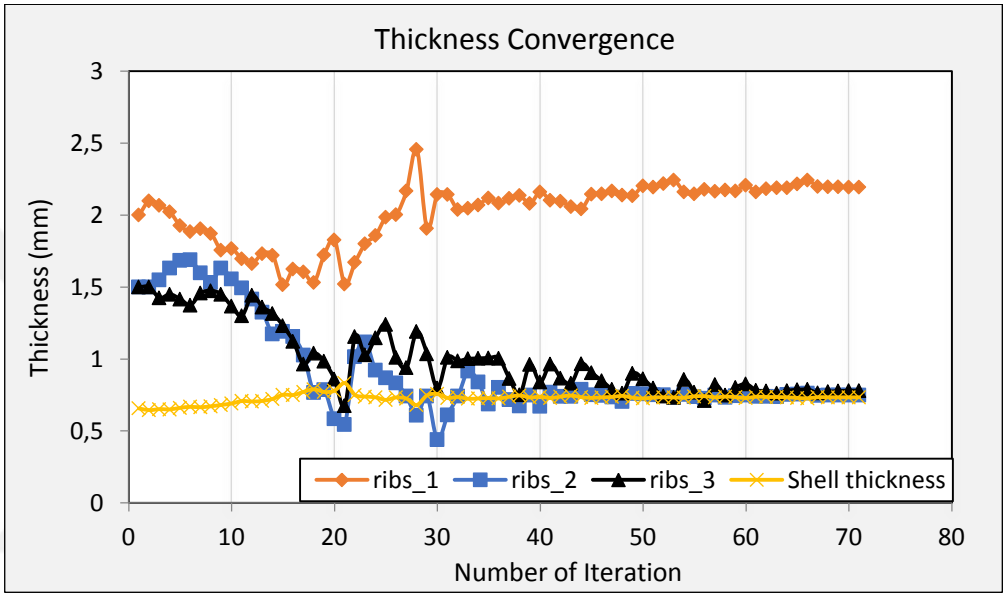

Figure 5.16. Iteration values of the design variables and the shell thickness

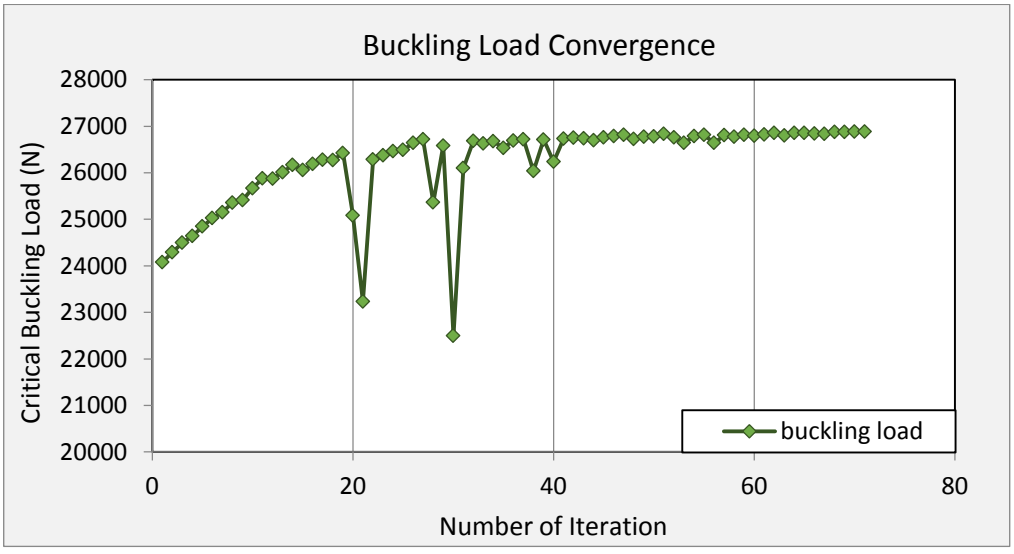

Figure 5.17. Iteration values of the objective function (critical buckling load)

The final geometrical details of the stiffened cylinder are given in Table 5.3. The stiffeners' heights are given after subtracting the shell thickness from the optimum values of the design variables. For example, the optimum shell thickness is 0.734 mm and it is subtracted from the converged value of ribs_1, which is 2.194 mm, to find the actual stiffener height of ribs_1. The obtained value is 1.460 mm. Since the difference between the shell thickness, 0.734 mm, and the converged values of other two groups of stiffeners, ribs_2 and ribs_3, is very small, the actual height of those two groups are neglected.

Table 5.3. The dimensions of the optimized stiffened cylinder.

	Dia. (mm)	Length (mm)	Shell thickness (mm)	Ribs_1 (mm)	Ribs_2 (mm)	Ribs_3 (mm)	*D/t*	*a* (mm)	*b* (mm)	Mass (gr)
Stiffened geometry	40	80	0.734	1.460	-	-	54.5	10	10	22.3

Force versus end shortening curve is given in Figure 5.18. as well as von Misses stress plots corresponing to the points indicated on the graph.The buckling load capacity of the optimum stiffened cylinder is 26885 N, which shows 22% increase compared to 22051 N buckling strength of the reference unstiffened cylindrical shell. Comparing the stress distribution in the optimum stiffened shell with that of the unstiffened shell at points A, B, C indicated on the graphs in Figures 5.18. and 5.3, it is observed that stiffeners help to distribute the structural stress around the cutout and stress accumulates in wider area until collapse occurs.

Figure 5.19. shows tha buckled shaped of both stiffened and unstiffened geometries. Total defermation of unstiffened shell is higher as it is observed but mostly towards to *y* axis at the middle section however, end shortening at the top edge (deformation at *z* axis) is higher for stiffened geometry.

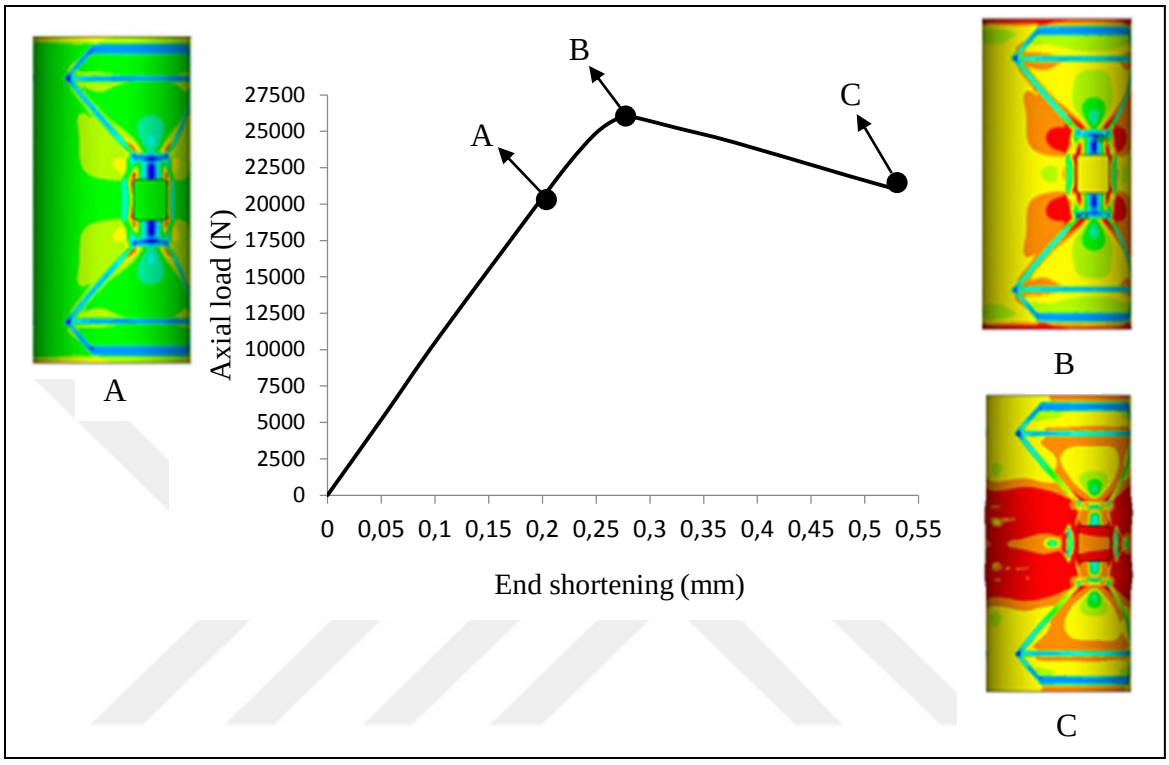

Figure 5.18. End shortening vs. load curve for optimum stiffened geometry with von Misses stress plots corresponding three points on the curve (A, B and C), *D/t*= 54.5, *L*=2*D*

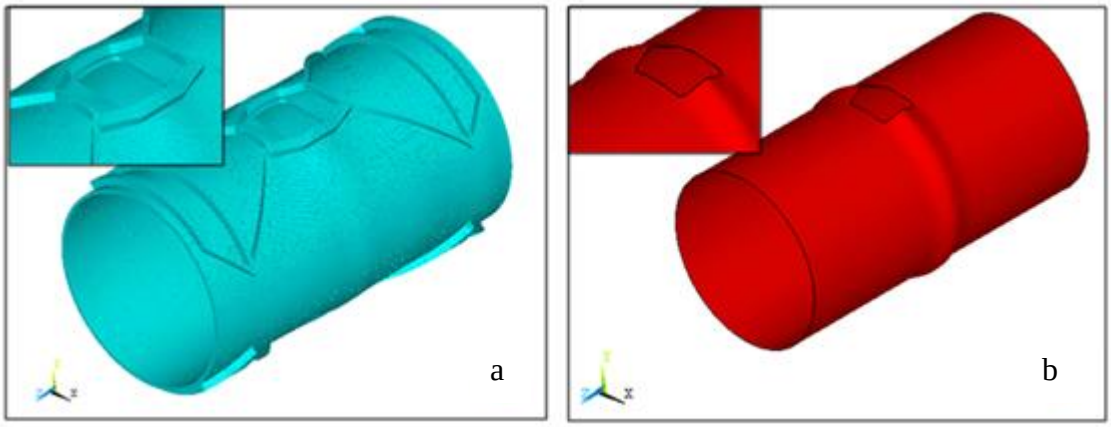

5.19. Buckled shape (a) stiffened geometry, (b) unstiffened geometry

6. DISCUSSION

The unstiffened geometry represents the reference cylindrical shell with no stiffeners on its surface. On the other hand, for the stiffened shell, the optimum stiffener pattern is found based on topography optimization and the heights of the stiffeners are optimized using a local search method. All dimensions of the two geometries are given in Table 6.1. Nelder-Mead optimization study shows the critical stress accumulated locations such as near the cutout have to be supported with stronger stiffeners. Because the presence of the cutout significantly affects the buckling load capacity.

Table 6.1. Dimensions of stiffened and unstiffened (reference) geometries

	Dia. (D) (mm)	Length (L) (mm)	Shell thickness (mm)	Ribs_1 (mm)	Ribs_2 (mm)	Ribs_3 (mm)	*D/t*	*a* (mm)	*b* (mm)	Mass (gr)
Unstiffened Shell	40	80	0.889	-	-	-	45.0	10	10	22.3
Stiffened Shell	40	80	0.734	1.460	-	-	54.5	10	10	22.3

Optimization results based on nonlinear analyses show that the shell thickness and the height of the main group of stiffeners, ribs_1, make great contribution to buckling strength of the structure. Thus, Nelder-Mead algorithm tries to make those two parameters as high as possible. Contrary to the topography optimization, which uses linear buckling analysis as its subcase, the height optimization shows that there is no need for stiffeners on the side surface. The reason is that Nelder-Mead optimization uses nonlinear buckling analysis as its subcase that takes into account material and geometrical nonlinearities. Geometrical imperfections cause significant decrease of buckling load as it is observed during 21th and 30th iterations when one of the stiffener's height goes below the shell thickness in Figure 5.20., the corresponding buckling load at those iterations decreases dramatically.

Nelder-Mead optimization biases the stiffeners near the cutouts to increase the buckling strength. Also, another critical location called “elephant food location,” where largest deflection occurs towards positive *y* direction during the buckling analysis, is supported with stiffeners. The connection between those two locations helps to distribute stress along the stiffeners.

Nonlinear buckling analyses in ANSYS are performed for both geometries and considerable increase is observed for the stiffened geometry compared to the reference geometry in terms of buckling load capacity. Additionally, numerical analyses provided valuable insight into post buckling behavior of the shells. Load versus end shortening curves extracted from the nonlinear buckling analyses of both geometries are given in Figure 6.1, in which point A represents the end point of the linear part of the curve, point B is where buckling occurs, and point C is the collapse point. The first observation is that both geometries have similar behavior until reaching the limit load for buckling. With the help of stiffeners, the structure provides more resistance against buckling and while its load-carrying capacity increases, the allowable deformation corresponding to the first buckling point also increases. It is observed that when the critical buckling load reaches to the level of 26885 N for the stiffened shell, the end shortening value reaches 0.28 mm according the nonlinear analysis results. The allowable shortening of the structure until collapse occurs increases due to the stiffeners. While buckling load capacity increases up to 22%, the allowable deformation of top edge of shell along *z* axis increases up to 14% without weight increase comparing with reference shell.

Linear buckling analyses were also conducted for both geometries. According to result, buckling load factor increased from 305 to 466 which mean structural strength of shell against to buckling increased 52.7%. In order to convert buckling load factor to critical buckling load, load factors are multiplied by applied load which was 252 N. In this case critical buckling load is found 117432 N for stiffened shell. While linear buckling analyses pointed 117432 N for critical buckling load of stiffened shell, nonlinear analysis show 26885 N so the ratio is 4.36 which was 3.5 for unstiffened reference shell.

Evaluating the post buckling curve of reference geometry in Figure 6.1, it simply behaves like imperfect unstable symmetric structure due the reason of having cutouts on its both sides. Generally, negative slope is expected from imperfect structures however, having stiffeners provide additional strength around the cutout which decreases structural imperfection and the result of this, negative slope goes towards to positive direction with stiffened geometry.

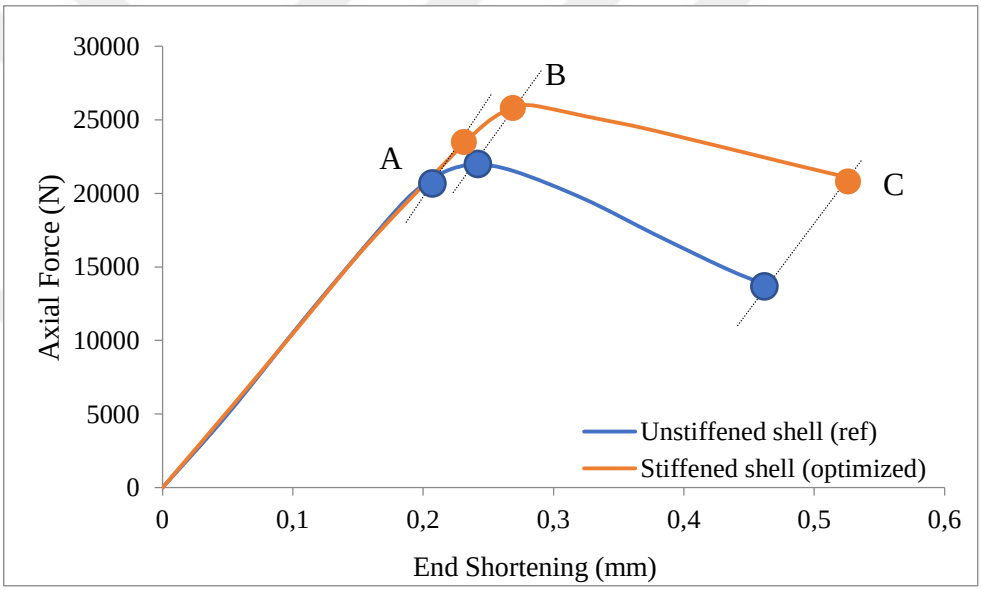

Figure 6.1. Comparison of force versus end shortening curves for both stiffened and unstiffened geometries

7. CONCLUSIONS AND FUTURE WORKS

In this study, the buckling load capacities of moderately thick stiffened and unstiffened cylindrical shells with cutouts are investigated numerically using ANSYS software. The FE model for an unstiffened cylindrical shell with a cutout is validated by comparing its predictions with the results reported by Han.et al. [2]. Topography optimization is performed to find the optimum stiffener pattern over the shell surface that maximizes the buckling strength using OPTI-STRUCT software. The optimization process produces a non-uniform stiffener pattern over the shell surface; larger stiffeners round the cutouts and near the top and bottom edges, but smaller sized stiffeners away from these regions. Stiffeners are particularly placed on locally high stressed regions.

After optimizing the stiffener pattern, the heights of the stiffeners and the shell thickness are optimized using Nelder-Mead optimization method. According to the results, stiffeners should be placed only around the cutouts and near the edges to recover the structural strength weakened due to the geometrical imperfection. As opposed to the first level optimization results, where stiffeners are generated almost all over the shell surface, in the second level optimization, no stiffeners are generated on surfaces away from the cutouts and the edges. This difference may be attributed to the use of linear buckling analysis in the first level and nonlinear analysis in the second. Besides, there is a significant difference between the buckling loads evaluated via linear and nonlinear analyses. While the critical buckling load increases up to 22% according to the nonlinear analysis, if the optimal stiffened shell is used, it increases 53% according to the linear analysis, but nonlinear analysis result is more reliable considering the correlation with experiment.

After the final configuration of stiffeners is determined, stiffener width optimization can be considered to make use of stiffener even better. Also, considering that only the numerical model for an unstiffened shell with a cutout is validated with experimental results, conducting an experimental study on the buckling behavior of stiffened cylindrical shells would be significantly valuable to understand effects of stiffeners on shell structures in realty.

REFERENCES

1. J. F. Jullien, A. Limam, "Effects of opening of the buckling of cylindrical shells subjected to axial compression,"*Thin-Walled Structures*, Vol. 31, pp. 187-202, 1998.

2. Haipeng Han, J. Cheng, F. Taheri, N. Pegg, "Numerical and experimental investigations of the response of aluminum cylinders with a cutout subject to axial compression," *Thin-Walled Structures*, Vol. 44, pp. 254-270, 2006.

3. T. Weller, J. Singer, "Experimental studies on the buckling under axial compression of integrally stringer-stiffened circular cylindrical shells,"*Journal of Applied Mechanics*, 1977.

4. E. Hotala, L. Skotny, "Experimental investigations on stability of stiffened cylindrical shell of steel silos,"*Journal of Constructional Steel Research*, Vol. 96, pp. 81-94, 2014.

5. S. Hui-shen, Z. Pin, C. Tie-yun, "Buckling and post-buckling of stiffened cylindrical shells under axial compression,"*Applied Mathematics and Mechanics*, Vol. 12, pp. 1195-1206, 1991.

6. Y. Zhu, J. H. Dong, B. J. Gao, "Buckling analysis of thin walled cylinder with combination of large and small stiffening rings under external pressure," *ProdeciaEngineering*, Vol. 130, pp. 364-373, 2015.

7. P. Forys, "Optimization of cylindrical shells stiffened by rings under external pressure including their post buckling behavior,"*Thin-Walled Structures*, Vol. 95, pp. 231-243, 2015.

8. M. Bagherib, A. A. Jafari, M. Sadeghifar, "A genetic algorithm optimization of the ring stiffened cylindrical shells for axial and radial buckling loads, "*Arch Appl. Mech.*, Vol. 81, pp. 1639-1649, 2011.

9. M. Sadeghifara, M. Bagherib, A.A. Jafaric, "Multi objective optimization of orthogonally stiffened cylindrical shells for minimum weight and maximum axial buckling load, "*Thin-Walled Structures*, Vol. 48, no.12, pp. 979–988, 2010.

10. B. Wang, K. Tian, C. Zhou, P. Hao, Y. Zhen, Y. Ma, J. Wang, "Grid pattern optimization framework of novel hierarchical stiffened shells allowing for imperfection sensitivity, "*Aerospace Science and Technology*, Vol. 62, pp. 114-121, 2017.

11. Y. Zhao, M. Chen, F. Yang, L. Zhang, D. Fang, "Optimal design of the hierarchical grid-stiffened cylindrical shell structures based on linear buckling and nonlinear collapse analyses, "*Thin-Walled Structures*, Vol. 119, pp. 315-323, 2017.

12. K. Tian, B. Wang, K. Zhang, J. Zhang, P. Hao, Y. Wu, "Tailoring optimal load-carrying efficiency of hierarchical stiffened shells by competitive sampling, "*Thin-Walled Structures*, Vol.133, pp. 216-225, 2018.

13. P. Hao, B. Wang, K. Tian, G. Li, K. Du, Y. Luan, "Integrated optimization of hybrid stiffened shells based on sub-panel elements, "*Thin-Walled Structures,* Vol. 103, 171-182, 2016.

14. T. G. Ghazijahani, H. Jiao, D. Holloway, "Structural behavior of shells with different cutouts under compression", Journal of Constructional Steel Research, Vol. 105, page 129-137, 2014.

15. A. Alsalah, D. Holloway, T. G. Ghazijahani, "Recover of capacity lost due to openings in cylindrical shells under compression, "*Journal of Constructional Steel Research*, Vol. 137, pp. 169-179, 2017.

16. P. Hao, B. Wang, K. Tian, G. Li, K. Du, Y. Luan, "Integrated optimization of hybrid stiffness stiffened shells based on sub-panel elements," *Thin-Walled Structures*, Vol. 103, pp. 171-182, 2016.

17. P. Hao, B. Wang, K. Tian, H. Liu, G. Li, Y. Wang, F. Niu, D. Zeng, "Simultaneous in buckling design of stiffened shells with multiple cutouts, *"Engineering Optimization*, Vol. 49, pp. 1116-1132, 2017.

18. S. Kim, C. Kim, "Buckling strength of the cylindrical shell and tank subjected to axially compressive loads,"*Thin-Walled Structures,* Vol. 40, pp. 329-353, 2002.

19. Altair, *"*Optistruct*", Hyperwork 12.0 User's Manuel, 2016.*

20. N. Mallon, R Fey, H. Nijmeijer, "Dynamic stability of a case excited thin cylindrical shell with top mass", Vol. 12, pp. 32-38, 2015.

21. ANSYS, "Shell-181", 16.0 User's Manuel, 2017.

22. GE Aviation, *ATP J. Engine*, 2016, https://www.euro.cz/byznys/cesko-posiluje-v-letectvi-ge-aviation-roztaci-novy-motor-1392907/galerie?id=284787, accessed at December 2018.

23. J. Cantarella, "Nelder-Mead Proof", *Numerical Optimization*, 2016.

24. Stresses in Engineering Components, *Physics Lecture*, pp. 43-46, Queen's University at Kingston, 2002, https://www.physics.queensu.ca/~lynann/lectures/W2L3.pdf, accessed at December 2018.

25. M. I. Elso, *Finite Element Method Studies on The Stability Behavior of Cylindrical Shells Under Axial and Radial Uniform and Non-Uniform Loads*, University Research Project, Hochschule Niederrhein University of Applied Sciences, 2012.